Development and Implementation of Diagnostics for the CLEAR Facility

01/04/18-31/08/18

CERN-THESIS-2018-403
//2018

Supervisors at PHELMA :
Elsa MERLE-LUCOTTE
merle@lpsc.in2p3.fr

Jean-Marie DE CONTO
deconto@lpsc.in2p3.fr

Hélène GUÉRIN
3rd Year - GEN
heguerin@cern.ch

Supervisors at CERN :
Wilfrid FARABOLINI
Kyrre Ness SJOBAEK

Summary

ANNEXES

List of Figures

List of Tables

Acknowledgments

At first time I would like to express my gratitude to *Roberto CORSINI* for having welcomed me in the LAT group and invited me to join the CLEAR operation group. A thankful acknowledgment to the whole LAT section too, and the other colleagues that I met during my period here, all of them let me feel welcome since the beginning.

Many thanks to *Elsa Merle-LUCOTTE* and *Robert FROESCHL* for the letters of reference that they provided me for this applications to the Technical Student Program. This first experience on an accelerator facility fully filled my expectations and still increases my curiosity to continue my career into particle accelerators world.

I would like to thank the teaching teams of the nuclear engineering branch of Grenoble INP - PHELMA, and of the JUAS master. Those two formations guided me to start my career in this field mixing physics and engineering, and I feel fully prepared to start working in it.

I also would like to thank *David AMORIM*, *Felix SOUBELET* and *Axel POYET* for their support and help in my orientation choices. They 3 achieved to convince me how amazing life at CERN can be (even and mostly working life). I strongly believe CERN will soon host new students from PHELMA. I am giving my best to represent the formations I come from and would be pleased to recommend them to anyone.

It would be hard not to thank the organization team of the Technical Student Program, which is definitely giving its best to make us enjoy as much as possible our stay at CERN.

I want to express my deepest gratitude to all the CLEAR operators, engineers and users that I met during my stay. All of you showed me how exciting it can be to operate such a machine.

Last but not least, I would like to thank *Wilfrid FARABOLINI* for all his support and his fatherly advices all along these 5 months at CERN. You proved me how necessary it is not only to understand physics, but to be able to deal with electronics, mechanics, optics and all this general engineering skills to run a machine such as CLEAR. Many thanks also to you *Kyrre SJOBAEK* for all your patience your help and your support during all these months. The CLEAR facility is really lucky and can be proud to have you both.

Glossary

Vocabulary

Damping time: Parameter defined to quantified the time required by an electronic system to react to the end of a perturbation.
Dark current: Particles extracted from the cathode due to the fields in the RF gun close to it. Particles from this current can transported downstream the accelerator.
Deflecting Cavity (Deflector or crab cavity): RF cavity deflecting the beam. The particles passing through are given a correlation between their transverse and longitudinal coordinates.
Dipole: Magnet used to bend the particles trajectory.
Dispersion: Beam parameter representing a change in a particle transverse position with a fractional momentum offset. **Dispersive** elements are accelerator components introducing dispersion.
Git: Free, open source and widely used control system designed to track changes in programming projects.
Good Field Region: Region in the gap of magnet where the field density is guaranteed.
Emittance: Measure of the average spread of particle coordinates in position-and-transverse momentum phase space.
Klystron: Electron tube that amplifies microwaves by velocity modulation.
Lattice: Ordered list of the accelerator magnets (optical components).
Magnetic length: Length of the trajectory of a nominal energy particle inside a magnet.
Matching section: Section composed of quadrupoles aiming at matching the transverse beam parameters to the desired ones.
Pockel cell: Voltage-controlled wave plates, used to rotate the polarization of a beam that passes through. A pair of Pockel cells is used to "chop" the laser for the photoinjector in time
PyQt: Toolkit framework used to extend Python language with features like GUI, signals and slots.
Quadrupole: Magnet used to focus the beam on one transverse plane, while defocusing in the other.
Repetion Rate: Duty cycle frequency.
Shunt Impedance: Measure of the strength with which an eigenmode of a resonant RF structure interacts with charged particles on a given straight line.
Train: Macro-pulse made of one or several bunches, and of which the size is defined by the duty cycle.
Transfer matrix: Matrix representing the action of an accelerator component on a particle's coordinates.

Acronyms

BCM: **B**eam **C**urrent **M**onitor:
BPM: **B**eam **P**osition **M**onitor.
CALIFES: **C**oncept d'**A**ccélerateur **L**inéaire pour **F**aisceau d'**E**lectrons **S**onde: probe test beam previously used in the CLIC test facility and readapted as an injector for the CLEAR facility.
CERN: European Organization for Nuclear Research.
CLEAR: **C**ERN **L**inear **E**lectron **A**ccelerator for **R**esearch.
CLIC: **C**ERN **LI**near **C**ollider: future international linear collider project.
CTF3: **C**LIC **T**est **F**acility 3: building previously dedicated to CLIC studies at CERN.
EOSD system: **E**lectro-**O**ptical **S**pectral **D**ecoding system: Method of measuring the bunch length.
GUI: **G**raphical **U**ser **I**nterface: type of user interface that allows users to interact with electronic devices through graphical icons instead of text interfaces.
HL-LHC: High-Luminosity Large Hadron Collider: Update of the LHC aiming to increase its luminosity.
ICT: **I**ntegrating **C**urrent **T**ransformer: device designed for bunch charge/current measurements.

I/Q modulation: "**I**n-phase" and "**Q**uadrature.": Signal modulation method using Cartesian coordinates instead of polar amplitude and phase data.
JAPC: **J**ava **A**PI for **P**arameter **C**ontrol: framework to build applications that control accelerator devices.
LINAC: **LIN**ear **AC**celerator.
OTR: **O**ptical **T**ransition **R**adiation: Light emitted when a fast charged particle is hitting a conducting surface.
RF: Radio Frequency.
rms: **r**oot **m**ean **s**quare.
S-BAND: RF band going from 2 to 4 GHz.
VESPER: **V**ery energetic **E**lectron facility for **S**pace **P**lanetary **E**xploration missions in harsh **R**adiative environments.
WFM: **W**ake **F**ield **M**onitor: Beam position monitors under development for the CLIC project, in order to preserve the emittance along the main CLIC linac.
YAG: **Y**ttrium Aluminium **G**arnet: synthetic crystalline material used for some beam diagnostics screens.

Introduction

Summer 2018 marks one year of operation of the CERN Linear Electron Accelerator for Research: CLEAR [1, 2]. Located in the Meyrin site of the European Organization for Nuclear Research (CERN), the facility has been developed in the building that was previously hosting the Test Facility CTF3 for the studies of the Compact LInear Collider (CLIC) project [3] held by CERN . After the successful end of the tests for this future linear collider project, the probe beam injector has been identified as relevant to build a new versatile electron linear accelerator as user facility. The project was adopted and the injector adapted for the new test beamline.

CLEAR is now operating as a stand-alone user facility, with the main purposes of being used for accelerator components R&D, general research and education motivations. Both laboratories, universities and internal users have shown their interest to conduct experiments on the facility. To be able to adapt to the variety of experiments and their requirements, CLEAR has to show its versatility over a wide range of tunable beam parameters.

For this purpose, CLEAR's operators and engineers are developing and improving a set of beam diagnostics, with the aim of setting with the best possible precision, the parameters required by the users.

This report aims to summarize some of the beam diagnostics calibrations and improvements that have been achieved since April 2018 and during the summer 2018 shutdown.

A brief description of the facility comes first, followed by the implementation of a user interface for bunch length measurement using a radio frequency deflecting cavity. The calibration of the dipole spectrometers calibration is then described, as well as an investigation of the current state of the Beam Position Monitors (BPMs) setup.

1 CLEAR, a versatile facility for research

CERN is currently hosting several experimental facilities in order to conduct research on accelerator components and future accelerator projects. CLEAR is one of these facilities. This section aims to present the LINAC and its beamline through their layout and beam parameters.

Figure 1.1 shows how the room of the previous CLIC test facility that has been chosen to host CLEAR (dark rectangle). A large part of the material already installed for CLIC probe beam has been reused, namely the injector: CALIFES (Concept d'Accélérateur Linéaire pour Faisceau d'Electron Sonde) [4].

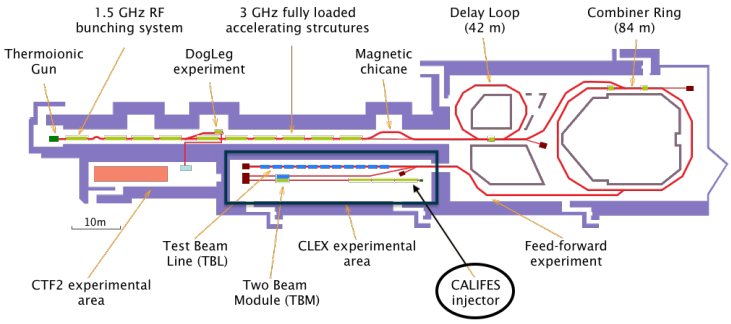

Figure 1.1: CLIC Test Facility building. The black rectangle indicates the room currently hosting CLEAR.

The first part of the facility is the injector, which is approximately 25 m long. Its layout is depicted in Figure 1.2, where the electron beam travels from right to left. Experiments mainly take place on the 16 m long beamline following the injector, and described in Figure 1.3.

1.1 The injector and beam parameters

The electron beam is produced from a photo-cathode on which is pulsed a UV laser [5]. Each hit of the laser extracts electrons from the cathode. Electrons are then accelerated through a RF-gun, which is equipped with an auto-regeneration chamber for the cathode coating. Inside the gun, the beam is structured into packets of particles called bunches. The bunch length can be tuned here from 300 µm to 1.2 mm rms. Three accelerating structures of a total length of 4.5 m come next, bringing the beam to its top energy. The first one is called the buncher.

In order to focus the beam and compensate the space charge, the gun, buncher and first accelerating structure of the LINAC (LINear ACcelerator) is placed in a tunable solenoid field. The injector line ends with a matching section containing 3 adjustable quadrupoles, and a spectrometer line.

In addition, the injector is widely furnished with beam diagnostic equipment:

- The beam coming out of the RF-gun is characterized with an Integrated Current Transformer (ICT) and a ceramic screen;
- Several Beam Position Monitors are positioned along the linac;

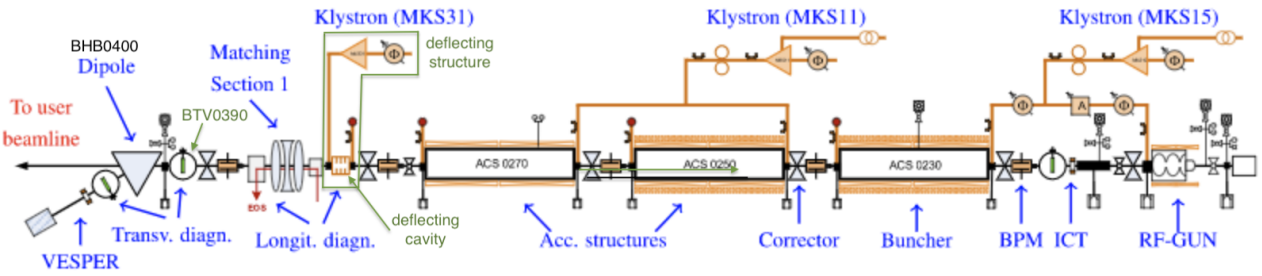

Figure 1.2: Layout of the CLEAR injector. The electron beam travels from right to left.

- An Electro-Optical Spectral Decoding (EOSD) system, streak camera measurements and a S-BAND (3 GHz) RF deflector allow for bunch length measurements;
- Before the spectrometer line, the transverse beam profile is determined thanks to an Yttrium Aluminium Garnet (YAG) scintillating screen and an Optical Transition Radiation (OTR) screen;
- The same system is also installed in the spectrometer line to enable beam energy measurements.

Regarding the RF system, the two accelerating structures, and the buncher and the RF-gun are powered with 2 independent 3 GHz klystrons (MSK15 and MSK11), which are equipped with a pulse compression system. This compression system allow pulse length and power tuning.

A 4.5 dB splitter divides the power from MKS15 between the RF-gun and the buncher. Two independent in-waveguide phase-shifters enable to adjust the phase of the RF signals delivered to these devices. The amplitude delivered to the RF-gun is also tunable using a variable attenuator. After the MKS11 klystron and its pulse compressor, a 3 dB splitter powers the two accelerating structures. A last klystron powers the transverse deflector located before the Matching Section 1. The design parameters are summarized in the Table 1.1, which reflects CLEAR's versatility.

Beam parameter	**Value range**
Energy	60 - 220 MeV
Bunch charge	0.001 - 1.5 nC
Normalized emittances	1 µm for <5 pC/bunch 20 µm for 20-100 pC/bunch (in both planes)
Bunch length	0.3 mm - 1.2 mm
Relative energy spread	< 0.2 % rms (< 1 MeV FWHM)
Repetition rate	0.833 Hz - 10 Hz
Number of bunches per train	between 1 and ≃200
Bunch spacing	1.5 GHz

Table 1.1: Beam parameters at the end of the LINAC [4].

1.2 The experimental beamline

The beamline layout is represented on Figure 1.3 and shown on Picture 1.4. It is divided into 7 parts.

The beam coming from CALIFES injector first meets another matching section. The following 2 m long section is dedicated for beam instrumentation tests. CLIC Test Stand comes next and is currently used for BPMs and Wake Fields Monitors (WFMs) studies. It hosts an accelerating cavity and 3 cavity BPMs, whose transverse position is remotely adjustable. One older cavity BPM of the same type is also installed as reference.

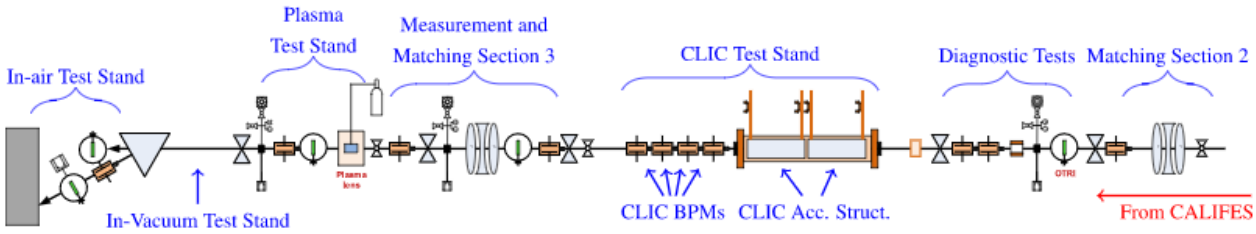

Figure 1.3: Layout of the CLEAR beamline. The electron beam travels from right to left.

The third matching section allows to fit the beam for the following plasma test stand, which is dedicated to a plasma lens experiment [6, 7]. Downstream this area are located two quadrupoles for matching to the in-air test stand and measuring the emittance after the plasma lens experiment through quadrupoles scans. Last comes the spectrometer line, and at the end of the line, a 1 m long area remains free to host experiments which do not require in-vacuum operation. Equipment for THz radiation studies are currently installed.

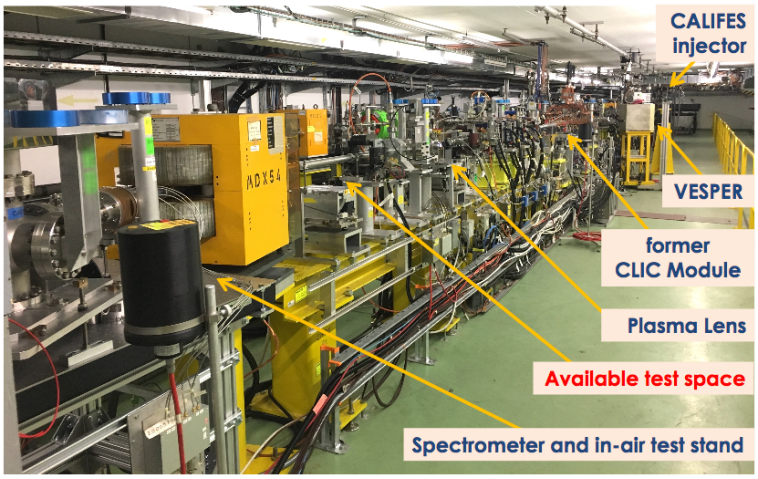

Figure 1.4: Picture of the CLEAR beamline (November 2017), captioned from the end of the line. (credit: Bruno Cassany)

From the experiments held on spring 2018, irradiations for medical dosimetry R&D were requiring very short bunches, below 1 ps. Efforts have been made before the users arrival to achieve this bunch compression. On the opposite, emittance growth in plasma studies took place later on the plasma lens experiment, using bunch length from 1 to 4 ps.

Conclusions

In summary, CLEAR stands for a versatile user facility. The hosted experiments require a wide range of beam parameters and lead the facility development. To control these parameters, large amounts of beam diagnostics are installed all along the machine.

2 Bunch length measurement

Longitudinal beam diagnostics at CLEAR are performed using a vertical radio frequency (RF) deflecting cavity (also called deflector). By observing its effect on the beam through the BTV0390 screen located downstream, one can deduce the bunch length. A Graphical User Interface (GUI) has recently been developed to improve this measurement.

This section aims to detail the measurement method theory before describing the software tool developed. All the sizes considered here are 1σ of the Gaussian shape of the bunch.

2.1 Deflector bunch length measurement: theory of the method

Equipments used for the bunch length measurement are indicated in green on Figure 1.2. The deflecting cavity is a TM_{110} mode cavity, operating at the same radio frequency as the whole LINAC (i.e. synchronized with the passage of the bunches). The 3 GHz klystron powering it is equipped with a phase shifter and an input power attenuator. These make it possible to tune the time profile of the field inside the cavity, which is shown on Figure 2.1.

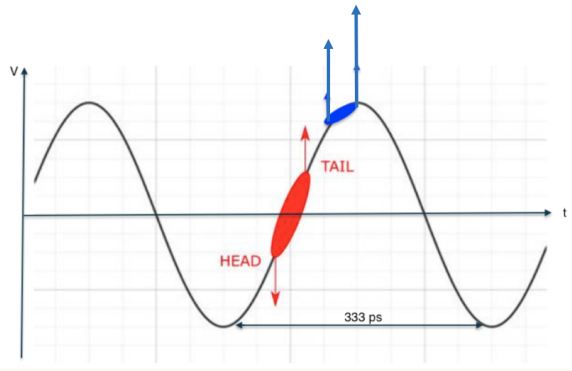

Figure 2.1: Deflecting voltage time profile inside the deflecting cavity and its effect on a bunch when phase is at zero-crossing (red bunch), and when not (blue bunch).

When a finite size bunch passes through the cavity, the particles perceive a kick proportional to the voltage. In this way, a bunch arriving nearby a field maximum (cf. blue bunch and arrows on Figure 2.1) will mainly be vertically kicked, whereas a bunch passing at the zero-crossing phase of the field will only be tilted (cf. red bunch and arrows on Figure 2.1) as head and tail see forces of opposite signs.

The bunch longitudinal shape, and notably the bunch length, can then be deduced from the transverse image of the beam observed downstream of the cavity. Figure 2.2 shows the shape of a round beam when passing through a cavity that is OFF, and its vertical spread caused by the cavity field when it is ON.

To ensure the best resolution measurement, the cavity phase must be at the field's zero-crossing, where the time derivative is maximum. The resolution can also be improved by increasing the voltage,i.e tuning the klystron power setting.

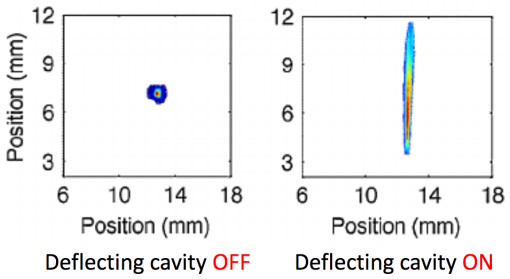

Figure 2.2: Image of the beam transverse profile seen on the camera 390 downstream of the deflecting cavity, with deflector OFF on the left, and ON on the right.

To compute the bunch length, one must quantify the kick effect of the cavity on the beam in the linear zone, which means calibrate the deflector. This step consists of measuring the beam vertical position for different phases in the linear zone, in the vicinity of the zero-crossing phase. A linear fit then provide the calibration coefficient k in mm/degree, which reflects the impact of the cavity field on the beam vertical position downstream.

Once the deflector has been calibrated, the vertical spot size measured at zero crossing phase $\sigma_{y,\mathrm{ON}}$ is the quadrature sum of the spot size measured without deflector $\sigma_{y,\mathrm{OFF}}$ and the spread (σ_y) caused by the bunch length (σ_z, cf. Equation 2.1). The bunch length can then be converted into time duration following Equation 2.2, where $f_{RF} = 2.998$ GHz is the operation frequency and k the calibration coefficient in mm/deg. The bunch in units of length σ_z $[mm]$ and in units of time σ_t $[ps]$ are linked with a factor which is the speed of light c, as stated in Equation 2.3.

$$\sigma_y\ [\mathrm{mm}] = \sqrt{\sigma_{y,\mathrm{ON}} - \sigma_{y,\mathrm{OFF}}} \tag{2.1}$$

$$\sigma_t\ [\mathrm{ps}] = \frac{\sigma_y\ [\mathrm{mm}]}{k\, f_{RF}\, 360^\circ} \tag{2.2}$$

$$\sigma_z\ [\mathrm{m}] = \sigma_t \cdot c \tag{2.3}$$

Depending on RF gun and accelerating structures voltage and phase settings, at the end of the LINAC, the bunch length is typically between 1 ps and 4 ps, that is in the range of [300 µm, 1.2 mm].

2.2 Scripts

Before the new software implementation, the deflecting cavity was already used for measuring the bunch length. The computation of the parameter was done by hand and the phase of the cavity was changed manually for the calibration. The objective of this new tool was to automatize the measurement and to make it faster, more precise, and less error-prone.

2.2.1 Language and programming tools

The new software had to be easy to handle and use for the operators, as well as accessible quickly from the control screens. A GUI thus had to be developed and implemented in the control panels common configuration nanager. These requirements lead to the choice of Python 3 as programming language to comply with the existing system. The GUI interactions with the user are handled with PyQt widgets and signals.

The bunch length measurement method needs to acquire many of data types from the several machine devices, making the software a data-driven application. The framework used at CERN to transfer signals from

the machine devices is JAPC (Java API for Parameter Control) [8]. Whenever it was possible, data processing and accelerator devices control programs have been developed as libraries, in order to allow their utilization to be used by other softwares. Libraries are structures in which functions and parameters are organized into classes. In this case, each library includes a main method which allows stand-alone execution. Its goal is to show how to use the classes and functions defined above, in order to make it easily reusable for other software developers. This type of structure is well fitting for scripts that are often needed in accelerator control softwares. Good examples are functions to interact with accelerator devices, as well as general data processing like the interpretation of an image received from a camera.

During its development, the scripts were stored on a Git repository [9], in order to allow the operators to use the new tools even during their implementation. Live feedback could be obtain in this way, and the operation was not disturbed by the software improvement. This also allows tracking of changes.

2.2.2 Programs structure

The GUI as shown on Figure 2.4 is on line since mid-Mai 2018 for live test with operators. The programs are structured as described on Figure 2.3.

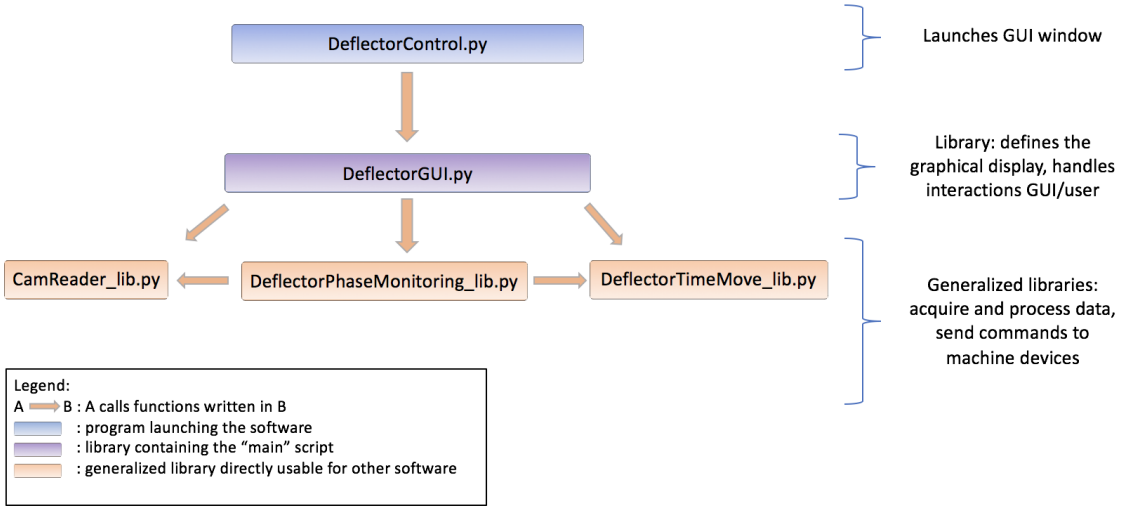

Figure 2.3: Organization scheme of the scripts.

The software is made up of 5 files, of which 4 are libraries.

A general script called `DeflectorControl` is the one to run for launching the software. It imports the general modules required, including JAPC and its settings, a module to interact with the interpreter, and one to create and handle the graphical interface. This script also calls the class written in `DeflectorGUI`, which is made as a library and controls all the GUI display, interactions with the user and calls the functions located in the 3 subordinate libraries (orange ones on Figure 2.3). These multi-purposes and interacting libraries correspond to the following goals:

- `DeflectorTimeMove_lib` allows to move the deflector RF signal on a large time scale. 2 preset time positions of the signals are considered as the ON and OFF states of the deflector mentioned in Section 2.1 and Figure 2.2.
- `DeflectorPhaseMonitoring_lib` contains 2 classes: The first one controls the phase of the deflecting cavity, and the second one contains all the functions required to calibrate the deflector, i.e. estimate its effect on the beam and determine the calibration coefficient.
- `CamReader_lib` acquires a given number of shots from a camera, and processes these images to read the position and the 1σ size of the beam spot.

Thanks to this program structure, once the software has been launched from the general control panel, the user can perform all the operations required to measure the bunch length directly from the GUI.

2.2.3 GUI presentation and user guide

Figure 2.5 shows the final version of the GUI panel, which is divided into 3 sections. This division corresponds to the steps to follow for bunch length measurement.

Figure 2.4: Graphical interface of the deflecting cavity control panel, as it was at the beginning of June 2018, after a bunch length measurement.

Figure 2.5: Graphical interface of the deflecting cavity control panel in its most recent version (summer 2018).

The first section, **Time**, uses functions defined in `DeflectorTimeMove_lib` library to move the cavity field in large time scale. The buttons "Move in" and "Move out" respectively synchronize and desynchronize the deflector signal with the beam passage, on the preset time positions mentioned in Section 2.2.2. The presence of the field inside the cavity is restricted in a time interval lead by 2 timing cursors that control the klystron pre-amplifier. The "Current timing" label above indicates the time position of the first cursor, and specifies if the cavity is "IN" time with the beam passage or not (mention "OUT"). The button "Move to time" also allows the user to manually chose when the field starts inside the cavity. For a proper use of the commands available in the next GUI section, the deflector signal timing should be "IN".

The **Phase** section is dedicated to phase manipulation of the deflector field. A label indicates the current phase that can be change either using the cursor, or the interval buttons applying $+/-10°$ or $+/-5°$ to the current phase, or even enter a given phase value in the dedicated text field. These buttons and the cursor are linked to functions from the "DeflectorPhaseChange" class written in `DeflectorPhaseMonitoring_lib` library. The purpose of this GUI section is to help finding a good phase interval to enter as input parameter for the deflector calibration step, which comes next. The user should find the largest phase interval for which the beam spot remains visible on the BTV0390 camera. The strength of the kick received by the bunches depends on the field's phase, but also on the deflector power. The latter can not be changed on-line from the control room, but can be tuned manually from the gallery by changing the attenuation between the klystron pre-amplifier and the klystron itself.

Last comes the **Measurements** section, using functions from the "DeflectorCalibration" class of the

`DeflectorPhaseMonitoring_lib` library, which itself calls functions from the two other data exploitation libraries. 4 inputs are required for the calibration: the 2 phase interval limits (buttons allow a final check of the beam spot position on the downstream camera), the number of steps, and the BTV0390 screen magnification. The latter is required for the conversion of the vertical sizes and displacements from pixels to mm. The number of steps fixes how many displacement measurements will be acquired for the calibration. Once the inputs have been specified, clicking on the "Start Calibration" button launches the calibration and the calculations. The deflector is automatically moved "OUT" in time to acquire the beam size without deflector. Then it is moved back "IN" and the calibration starts. For each measurement to acquire, the beam spot position is computed via `CamReader_lib` and averaged over 5 shots. The beam spot position and size determination is detailed in Section 2.3.1. A last spot size measure is done at the zero-crossing phase, and the bunch length is computed in time and length units. All the results finally appear on the GUI in the **Outputs** fields, and a new window shows the calibration curve. The reasonability of this curve should be controlled by the user.

2.3 Testing

Tested during one month of operation, the software could benefit from users feedbacks. Some improvements have been added, and some limits were also observed.

2.3.1 Improvements developed with testing

The software has been tested by both operators used to bunch length measurements with the deflector and external users. Recurrent crashes as well as main difficulties were reported, leading to some optimizations.

Beam position and size acquisition

`CamReader_lib` library has been dedicated to process the data coming from one camera in order to get the position and the size of the beam from this image.

Depending on the camera screen, the chosen filter, the beam intensity, etc., images can look significantly different. The poor reliability of the simple fits of the first versions was the source of many program crashes.

After improvements, several stages now lead to the acquisition of these parameters. The four square corner areas of the image are first compared in order to subtract the background, which is assumed to be flat. Then the pixel intensities are projected along each axis, creating two projection vectors for the transverse dimensions x and y. For each one, a first Gaussian fit is applied to obtain initial values of the spot size and position, respectively corresponding to the standard deviation and the peak of the fit. A region of interest is then defined at +/-2σ around the position, and an second fit is done in this region. This gives the final position and size parameters. Figure 2.6 illustrates this. The process is repeated for a given number of consecutive shots, in order to average the beam parameters to find more representative values when the beam is not stable in time.

This library has thus been optimized to return the most descriptive beam parameters. An error message is displayed when the image quality is too bad for the fitting routine to work.

Time move of the deflector cavity signal

Other bugs were caused when the time position of the deflector cavity signal was manually displaced from small intervals. The two cursors have to be displaced one by one, avoiding a too long signal presence in the cavity, as this can cause the klystron to stop due to reflected power caused by arcs in the cavity and waveguide network. This kind of situations leads to 15 min of restarting time for it. This observation lead to an adjustment of the displacement method, tuning the steps size depending on the requested time gap.

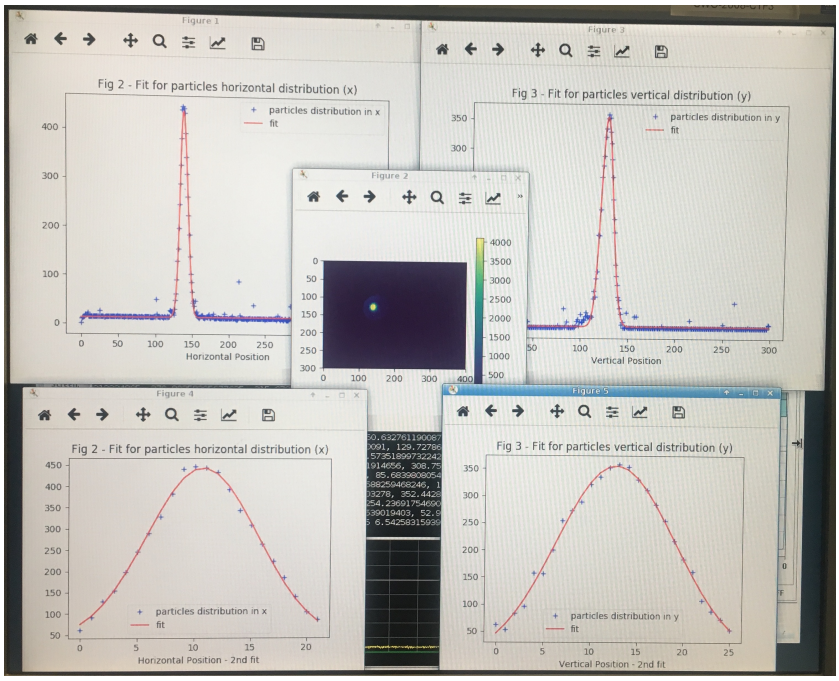

Figure 2.6: Determination of beam transverse positions and sizes on an image from camera BTV0390 (central figure, axis in pixels). The upper left and right figures respectively show in blue the projections on x and y axis of the pixels light intensities. The red curve corresponds to the first Gaussian fit. Figures at the bottom left and right respectively show the x and y projection of these pixel intensities in the 4σ large region of interest and the second Gaussian fit applied to this region. Projections abscissa scales are in pixels and ordinates ones in light intensities (arbitrary units).

GUI simplification

Comparing the first version of the GUI on Figure 2.4 and the current one on Figure 2.5, significant simplifications have been made.

The measurement had to become as user-friendly as possible. The initial **Calibration** and **Measurements** parts have been merged. One button now ensure the calibration and all the measurements this step requires, as well as outputs computation and display. The field to provide the screen magnification has been replaced as well by selection buttons. From the very first versions, buttons to quickly change the phase by fixed typical steps were also added.

2.3.2 Limits & foreseen improvements

During the test time, some limits have also been observed. The most commom reported issues concern non-Gaussian bunch profiles.

Non-Gaussian profiles short bunches

In particular when bunches are compressed down to below 1.5 ps, the longitudinal bunch profile loses its Gaussian shape, as shown on Figure 2.7. Due to bunch head-tail correlation in energy, the longitudinal shape of the particles distribution inside the bunch is not symmetric anymore and the Gaussian fit loses its significance. The two examples of Figure 2.7 show that in this case, transverse position and size of the beam spot observed on BTV0390 can be significantly far from the results returned by the Gaussian fitting process, leading to bunch length overestimation.

Above 1.5 ps bunch length, the time distribution recovers its Gaussian shape.

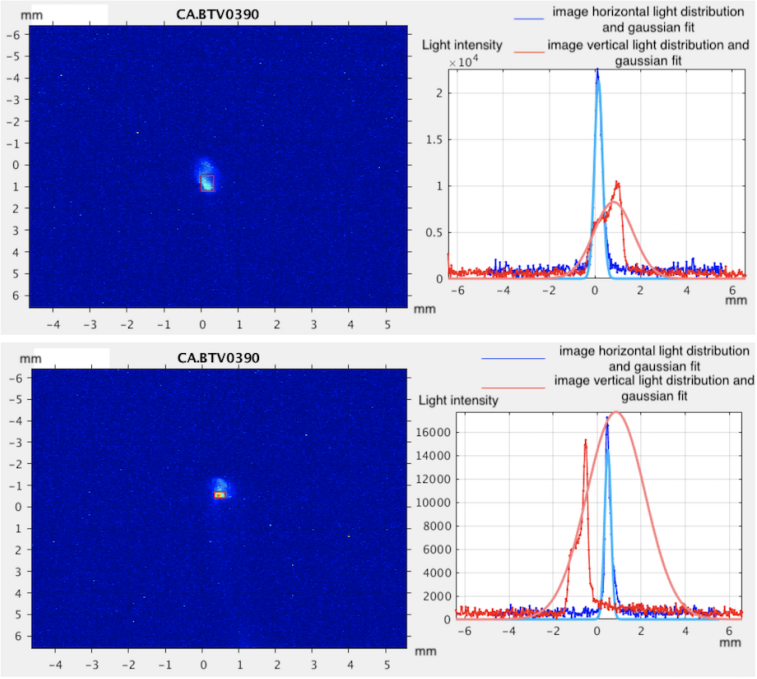

Figure 2.7: Two cases of images from BTV0390 with deflector ON, after bunch compression below 1.5 ps (left), and their beam spot projections and tentatives Gaussian fit (right). The red distribution (the one of picture vertical axis) represents bunch particles distribution in time. In both examples the corresponding tentative Gaussian fit is not representative and overestimates the bunch length.

To bypass this problem, another data processing scheme should be implemented for short bunches cases. One of the potential solutions raised would be to consider the full width at half maximum of the intensity peak instead of the Gaussian fit standard deviation for the spot size. A solution should also be found to determine the spot position, and some criteria should be defined to distinguish short bunches to treat separately.

In the meanwhile, this short bunch limit has to be kept in mind when using the deflector for bunch length measurements.

Uncertainties

Depending on the beam transverse position stability in time, the bunch length measurement can be more or less precise. Its precision is defined by the standard deviation derived from the 5 beam spot positions measurements obtained before their average from the different image shots. This amount may vary quite significantly depending on the laser stability (itself depending on parameters as temperature and so on). For the moment, no uncertainty appears on the GUI, but it could be easily added by considering the standard deviations of σ_y, OFF and σ_y, ON.

GUI operations status label

Another comment from users concerns the lack of feedback from the GUI during calibration and computation operations. Once the final button has been pressed, operations can last about 30 seconds without any sign showing that it is ongoing. The GUI updates once the total operation has been completed (like it does for deflector phase and time changes commands), but it stays frozen pending it.

A "Current status" label visible on Figure 2.5 has been added for this purpose, on the bottom of the GUI. The following field is supposed to tell which operation is ongoing, in particular during calibration

and bunch length computation steps. This solution is based on an "update_callback" function defined in `DeflectorGUI` script and global parameters passed each time one sub-library is called. However the GUI dedicated field only updates at the end of all operations, which does not solve the problem.

A solution considering the use of internal PyQt signals should be investigated, however this requires advanced knowledge of PyQt signal manipulation.

Conclusions

To conclude on this recent tool, the main objectives of allowing a fast and easy acquisition of the bunch length have been fulfilled. The new GUI permits to control the effect of deflector's field on the beam through its phase and time limitation control. The several fits applied in data processing steps guarantee the reliability of the final result and the display of the phase scan fit allows a control of its relevance. However short bunch length measurements are biased due to the non-Gaussian profile of the particle's time distribution in bunches below about 1.5 ps length. This limit has to be kept in mind for a proper interpretation of the software outputs. The GUI has been validate as easy to handle after improvements during a testing period. Live update of ongoing operations status can still be improved.

First uses of the software by present operators scientists were successful. Other bunch length measurement diagnostics are being developed on CLEAR and their results will be compared with deflector measures. Bunch length stability in time studies are foreseen to investigate laser and accelerating structure time stability and repeatability studies.

3 Calibration of energy spectrometers

As mentioned in the Table 1.1, CLEAR's LINAC has been designed in order to reach energies from 60 to 220 MeV. To measure this parameter, two spectrometer lines are installed on the whole facility: one at the end of the injector (cf. Figure 1.2), and the other at the end of the beamline (cf. Figure 1.3). Two identical dipoles [10] (shown on Figures 3.2 and 3.1) are thus placed to deviate the beam on the VESPER and in-air experimental platforms, where Yttrium Aluminium Garnet (YAG) screens are installed to determine the beam position, and thus energy.

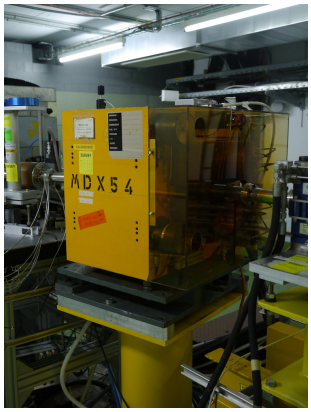

Figure 3.1: Dipole located at the end of the beamline, deviating the beam to the in-air experimental line.

Figure 3.2: Dipole located at the end of the LINAC, deviating the beam to the VESPER experimental line.

The computations aiming at making the spectrometers fully operational to accurately determine the beam energy have been done recently. This section presents these calculations, after having described the spectrometer energy measurement principle.

3.1 Principle of the method

Inside dipole magnets, a vertical magnetic field is produced thanks to the current circulating through the coils located above and below the vacuum chamber where the beam is passing.

When passing through a dipole, a charged particle perceives a Lorentz force which is deviating it in the horizontal plane. The deviation angle depends on the particle energy (or momentum), following the magnetic rigidity relation given in Equation 3.1. The magnetic rigidity and Equation 3.2 derive the particle's momentum P [MeV/c] as a function of the curvature radius ρ [m], and of the magnetic field density B [T] of the dipole.

$$B\rho = \frac{P}{q} = \frac{P\ [\text{MeV/c}]}{300} \tag{3.1}$$

$$P = 300\,B\,\rho \tag{3.2}$$

As electrons are traveling at hundreds of MeV, they can be considered as relativistic ($\beta \simeq 1$), justifying that $E \simeq Pc$ where c is the speed of light. Any particle having a different energy from the nominal one will be deflected with a different angle. A screen installed downstream of the dipole will then allow to determine the position x in the horizontal plane, to find the angle difference $\Delta\theta$, and finally to the energy deviation $\Delta E = E - E_0$ from the nominal energy.

Once the relation between the position on the screen and the corresponding energy difference has been derived ($x = f(\Delta E)$), it can be applied to determine the energy spread inside beam bunches.

This relation can be determined from beam optics theory. One interesting parameter to consider is the beam dispersion D. This directly links the beam horizontal position x (defined with respect to the nominal trajectory) with the momentum offset $\Delta p = p - p_0$ against the nominal one p_0.

$$x = D\frac{\Delta p}{p_0} \tag{3.3}$$

The spectrometer line can be decomposed into two elements: a dipole, horizontally deflecting the beam particles, followed by a drift space of length L, on which no force is applied to the particles. The impact of this system on the beam trajectory can be modeled using the so-called transfer matrix M_T as written in Equation 3.4. The particles are said to enter in the spectrometer system in a point A and exit in a point B. M_T defines how the beam dispersion D and its derivative over the trajectory coordinate s, $D' = \frac{\mathrm{d}D}{\mathrm{d}s}$, evolve between A and B.

$$\begin{pmatrix} D \\ D' \\ \frac{\Delta p}{p_0} \end{pmatrix}_B = M_T \cdot \begin{pmatrix} D \\ D' \\ \frac{\Delta p}{p_0} \end{pmatrix}_A \tag{3.4}$$

$$= M_{drift} \cdot M_{dip} \cdot \begin{pmatrix} D \\ D' \\ \frac{\Delta p}{p_0} \end{pmatrix}_A \tag{3.5}$$

This 3×3 transfer matrix can be decomposed into the multiplication of the transfer matrix corresponding to each of the lattice elements (namely one dipole followed by one drift space), as derived in Equation 3.5. The expressions of each element transfer matrix are given in Equations 3.6, where θ is the dipole's bending angle.

$$M_{drift} = \begin{pmatrix} 1 & L & 0 \\ 0 & 1 & 0 \\ 0 & 0 & 1 \end{pmatrix} \qquad M_{dip} = \begin{pmatrix} \cos\theta & \rho\sin\theta & \rho(1-\cos\theta) \\ -\frac{\sin\theta}{\rho} & \cos\theta & \sin\theta \\ 0 & 0 & 1 \end{pmatrix} \tag{3.6}$$

In CLEAR's lattice, no strong dispersive elements are located before the beam enters in one of the dipoles, so that the dispersion and its derivative in point A are zero. Further assuming that there is no momentum spread, that leads to Equation 3.7 and to the dispersion at the exit of the system, given in Expression 3.8.

$$\begin{pmatrix} D \\ D' \\ \frac{\Delta p}{p_0} \end{pmatrix}_A = \begin{pmatrix} 0 \\ 0 \\ 1 \end{pmatrix} \tag{3.7}$$

$$D = \rho(1 - \cos(\theta)) + L\sin\theta \tag{3.8}$$

Thanks to the dispersion which can be determines by considering the layout of the spectrometers (θ dependence) and the current circulating in the dipoles coils (for the bending radius ρ), a beam offset x observed on a screen at the end of the drift space can be linked to a deviation from the nominal energy.

3.2 Spectrometers layout

The spectrometers are installed as described on the Figure 3.3. In the first one, the beam coming at the nominal energy enters in the dipole with an angle $\theta_{400} = 17.5°$ and leaves the dipole perpendicularly to its output face.

The second dipole is placed so as the nominal energy beam both enters and leaves the dipole with half the total deflection angle, $\frac{\theta_{800}}{2} = 11.375°$.

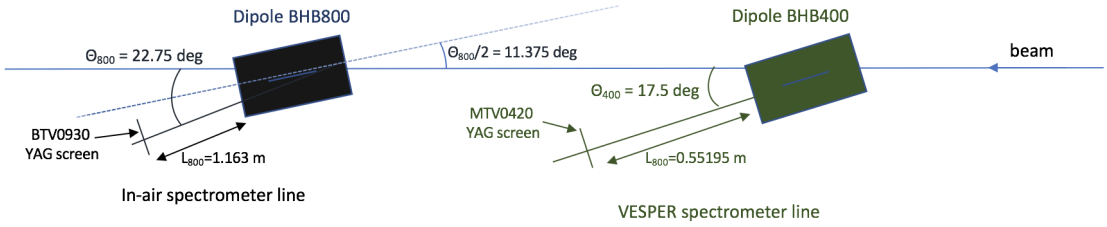

Figure 3.3: Layout of CLEAR's spectrometers.

3.3 Determination of the nominal energy

From the described layout, the beam has been measured experimentally at the center of the screen for currents of $I_{400} = 50$ A on VESPER's spectrometer, and of $I_{800} = 70$ A on the in-air spectrometer (nominal currents).

From the calibration of the dipoles that was done at their reception by CERN [11], the magnetic length of the magnets has been measured of $l_m = 0.4710$ m for a when using dipoles with currents in the range of 40-80 A circulating in their coils. The magnetic density in the good field region of the coils (which for both cases cover the particles trajectories) can also be determined as function of the magnet current, as shown on the graphic of Figure 3.4.

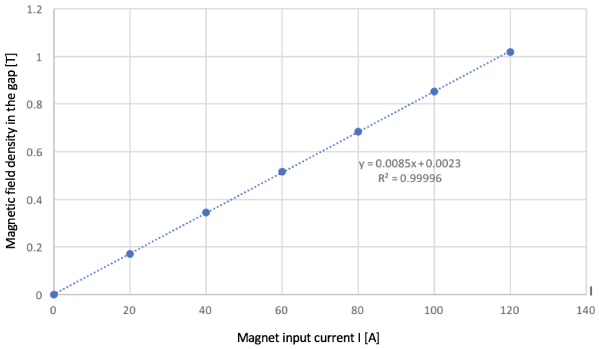

Figure 3.4: Evolution of the magnetic density B in the spectrometers dipoles as function of the input current I.

Geometrical considerations are required to obtain the link between the curvature radius and the magnet magnetic length l_m. Figures 3.5 and 3.6 describe both spectrometer geometries, where the dipoles are sketched as blue rectangles and the beam trajectory is shown in orange. From these schemes, the expressions of the curvature radius is $\rho_{400} = \frac{l_m}{\sin(\theta_{400})}$ for the VESPER dipole, and $\rho_{800} = \frac{l_m}{2\sin(\theta_{800}/2)}$ for the in-air one. When using the nominal currents in input of the spectrometer dipoles, the corresponding nominal energy E_0 (i.e. the one of a beam passing at the center of the YAG screens) is given by Equation 3.9.

The nominal energy of the in-air spectrometer is the typical range of energies used for the machine operation. VESPER's spectrometer energy of 161 MeV corresponds to the one set up for irradiation experiments that are taking place on this spectrometer line.

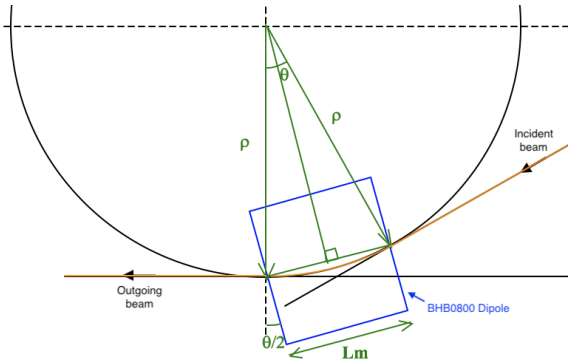

Figure 3.5: Scheme of the trajectory of the particle with nominal energy in in-air spectrometer line.

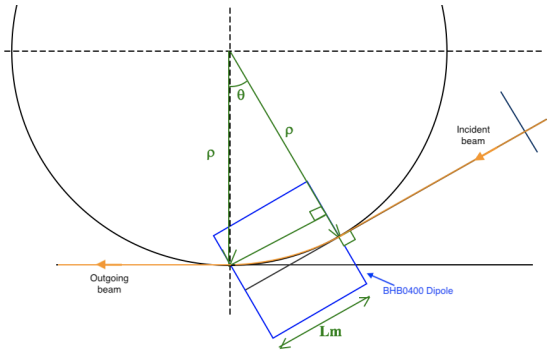

Figure 3.6: Scheme of the trajectory of the particle with nominal energy in VESPER spectrometer line.

$$E_{0,\text{VESPER spec.}} = 300\ [\text{MeV/c/m/T}]\ \frac{l_m}{\sin(\theta_{400})}(0.0085\ [\text{T/A}] \times I + 0.0023\ [\text{T}])\, c = 161\ \text{MeV} \tag{3.9}$$

$$E_{0,\text{in-air spec.}} = 300\ [\text{MeV/c/m/T}]\ \frac{l_m}{2\sin(\theta_{400}/2)}(0.0085\ [\text{T/A}] \times I + 0.0023\ [\text{T}])\, c = 214\ \text{MeV} \tag{3.10}$$

3.4 Energy of beam of transverse position deviation

From the beam optics introduction given in section 3.1, the link between the horizontal spot position seen on YAG screens and the beam energy can be derived by replacing the corresponding expression of the curvature radius for each spectrometer in Equation 3.8, and inserting the dispersion value in Equation 3.3. Relations 3.11 and 3.12 finally link the measured horizontal spot position x_{meas} on spectrometers screens (in pixels), and the beam energy.

$$E_{\text{VESPER spec.}}\ [\text{MeV}] = E_{0,\text{VESPER spec}}\left(\frac{x_{400,\text{meas}}\ [\text{pix}] \times 0.2488\ [\text{mm/pix}] \times 10^{-3}\ [\text{m/mm}]}{\frac{l_m}{\sin\theta_{400}}(1-\cos\theta_{400}) + L_{400}\sin\theta_{400}} + 1\right) \tag{3.11}$$

$$E_{\text{in-air spec.}}\ [\text{MeV}] = E_{0,\text{in-air spec}}\left(\frac{x_{800,\text{meas}}\ [\text{pix}] \times 0.1524\ [\text{mm/pix}]}{\frac{l_m}{2\sin\theta_{800}/2}(1-\cos\theta_{800}) + L_{800}\sin\theta_{800}} + 1\right) \tag{3.12}$$

From the screen sizes of 10 cm for BTV0420 and 6 cm for BTV0930, the minimum and maximum measurable energies are respectively of $E^{\text{min}}_{\text{VESPER}} = 127$ MeV and $E^{\text{max}}_{\text{VESPER}} = 195$ MeV for the VESPER spectrometer, and of $E^{\text{min}}_{\text{in-air}} = 202$ MeV and $E^{\text{max}}_{\text{in-air}} = 226$ MeV for the in-air spectrometer. Beams with such energies may however be affected by the size of the Good Field Region inside the dipole gaps.

3.5 Uncertainties and result cross check

The sources of errors for this energy measurement have been identified and quantified. They are listed as follows:

- Error in the magnetic length: $\sigma_l = \pm 1$ mm
- Misalignment in spectrometer beamlines: $\sigma_{\theta,400} = \pm 1.14°$ $\sigma_{\theta,800} = \pm 1.37°$

From the operators experience [12], the errors in the position determination and in the current reading are in this case negligible in comparison to the other error sources mentioned above, provided that the beam is not very unstable.

The final error estimation σ_E of the beam energy measurement is as derived in Equation 3.13, assuming that the errors on the magnetic length and on the misalignment estimation are Gaussian distributed and uncorrelated. The computation of the derivatives described in Equation 3.14 and calculated in Equations 3.15 to 3.18, leads the final precision for the energy measurement is $\sigma_{\mathrm{E},400} = 10.1$ MeV for the VESPER spectrometer, and $\sigma_{\mathrm{E},800} = 7.3$ MeV for the in-air spectrometer.

$$\sigma_E = \sqrt{\sigma_{E,l}^2 + \sigma_{E,\theta}^2} \tag{3.13}$$

$$\sigma_{E,l} = \frac{\mathrm{d}E}{\mathrm{d}l}\,\sigma_l \qquad \sigma_{E,\theta} = \frac{\mathrm{d}E}{\mathrm{d}\theta}\,\sigma_\theta \tag{3.14}$$

$$\sigma_{E,l,400} = \frac{300\ [\mathrm{MeV/c/m/T}]}{\sin(\theta_{400})}\,0.0085\ [\mathrm{T/A}]\cdot I_{400}\,\sigma_l = 0.339\ \mathrm{MeV} \tag{3.15}$$

$$\sigma_{E,l,800} = \frac{300\ [\mathrm{MeV/c/m/T}]}{2\,\sin(\theta_{800}/2)}\,0.0085\ [\mathrm{T/A}]\cdot I_{800}\,\sigma_l = 0.901\ \mathrm{MeV} \tag{3.16}$$

$$\sigma_{E,\theta,400} = -\frac{\cos(\theta_{400})}{\sin^2(\theta_{400})}\,300\ [\mathrm{MeV/c/m/T}]\cdot l_m\,0.0085\ [\mathrm{T/A}]\cdot I_{400}\cdot\sigma_{\theta,400} = -10.1\ \mathrm{MeV} \tag{3.17}$$

$$\sigma_{E,\theta,800} = \frac{\cos(\theta_{800}/2)}{2\sin^2(\theta_{800}/2)}\,300\ [\mathrm{MeV/c/m/T}]\cdot l_m\,0.0085\ [\mathrm{T/A}]\cdot I_{400}\cdot\sigma_{\theta,800} = 7.24\ \mathrm{MeV} \tag{3.18}$$

This error obtained for the measurement is relatively high but the method still provides a good order of magnitude of the beam energy with no more than 21 MeV uncertainty. The nominal energies finally read $E_{\text{VESPER spec}} = 160 \pm 10$ MeV and $E_{\text{in-air spec}} = 214 \pm 7$ MeV.

Conclusions

The computations to calibrate the two spectrometers screens have been done with a precision down to the tens of MeV, which reaches the operators expectations. A simple scaling system has been added on the horizontal axis of the spectrometers cameras in the dedicated Matlab GUI, to be able to read directly the beam energy from the live position of the beam spot. The two spectrometers are complementary with the range of energies that each one can measure: the VESPER spectrometer line allows measurements from 125 to 195 MeV, and the in-air one, measurements from 202 to 226 MeV.

4 Beam Position Monitors behavior investigation

For transport optimization purposes, a set of 6 cavity Beam Position Monitors (BPMs) [13] and 4 inductive BPMs [14] is installed on the beamline. Their main purpose is to estimate the charge and the center of mass of the beam. However they have not yet been calibrated. The transverse profile and position of the beam are currently estimated thanks to the screens placed along the machine. Beam charge can be measured by Integrating Current Transformers (ICT) located after the RF-gun, and on VESPER spectrometer line.

The BPMs signals acquisition setup is already operational. The objective of the following work is to investigate their behaviors with different bunch setups, try to explain them, and to determine how to effectively calibrate those devices to measure the beam parameters from these non interceptive diagnostics.

Descriptions of the 2 types of BPMs and their functioning are described first, followed by details of data acquisition conditions. The results are then introduced and analyzed, and the conclusions presented.

4.1 Description of the inductive BPMs

Inductive BPMs are located all along the experimental beamline and referenced as shown on Figure 4.1 by numbers corresponding to their position on the machine longitudinal axis: 520, 560, 780 and 820. These devices consist of a pick-up hardware installed around the beam pipe, and a front-end electronic device combining and amplifying the signals and sending them to a digitizing system.

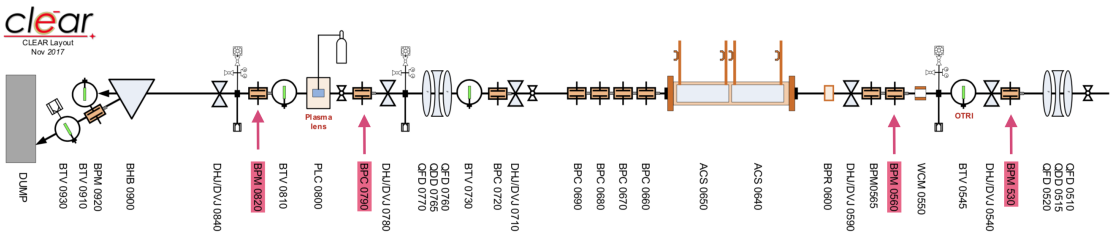

Figure 4.1: Location of the inductive BPMs studied along CLEAR experimental beamline.

4.1.1 Hardware description and functioning

Inductive BPMs as shown on Figures 4.2 and 4.3 sense the azimuthal image current distribution.

Figures 4.4 and 4.5 describe how a signal from a bunch passage is picked up with BPMs. When a charged bunch is passing through the beam pipe, it is creating an image current of the same magnitude and reversed polarity in the conductive walls around. In the case of bunched beam, this current intensity is varying in time and its conversion into a signal can provide informations concerning the beam longitudinal profile. The principle of a BPM is to pick up such signals via electrodes. Their amplitude being proportional to the bunch charge and proximity, informations concerning bunch charge and position can thus be deduced from well positioned electrodes.

In the case of inductive BPMs, a ceramic gap separates electrodes from the beam pipe's vacuum, the ferrite

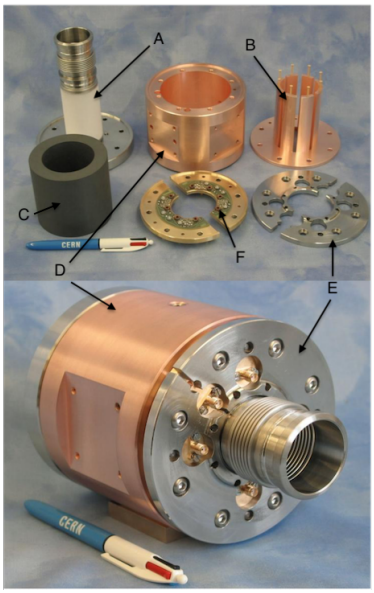

Figure 4.2: CLEAR inductive BPM components and assembly. The beam pipe is intersected with a titanium coated ceramic tube **A**. 8 copper electrodes **B** conduct the wall current to toroidal transformers **F** that are mounted on a electronic boards. A ferrite cylinder **C** is mounted around the copper strips and inserted itself in the housing **D**. The plates holding the electronic boards are connected to the electrodes thanks to screws passing through the transformers rings. The clamps **E** laterally tighten the plates with connectors screwed.

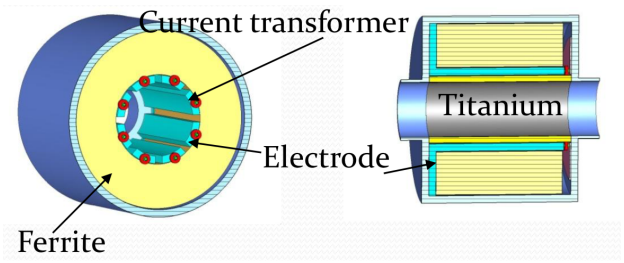

Figure 4.3: Scheme of CLEAR inductive BPMs.

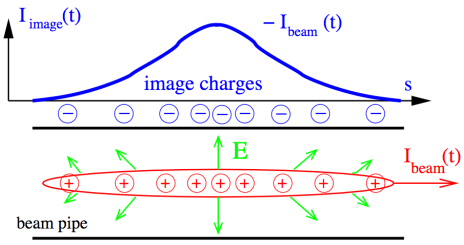

Figure 4.4: Wall current (blue) induced by a proton beam (red) passage in a beam pipe. The image current has the same magnitude but reversed polarity [15].

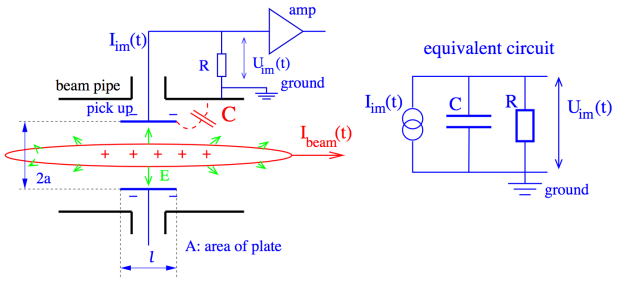

Figure 4.5: Scheme of a pick-up electrode and its equivalent circuit [15].

cylinder forces low frequency signals to the inductive strips, and the shield ensures protection from ground currents and noise. The image currents travel to reach the current transformers, which amplify the signals.

4.1.2 Signal acquisition

One output is dedicated to each electrode. Those outputs are then summed in pairs, as described on Figure 4.6, to form 4 signals: the two electrodes the closest to the right of the beam pipe gather in H_+, the two closest electrodes to the left of the beam pipe form H_-, and in the same way, V_+ and V_- are created for the vertical axis. An active hybrid circuit finally receives these signals, summing all of them to make a sum signal called

$\Sigma = H_+ + H_- + V_+ + V_-$, which is proportional to the beam current. The circuit also makes two difference signals $\Delta H = \frac{H_+ - H_-}{\Sigma}$ and $\Delta V = \frac{V_+ - V_-}{\Sigma}$, normalized by the sum signal. These horizontal and vertical difference signals are respectively proportional to the beam position in the horizontal and vertical axis.

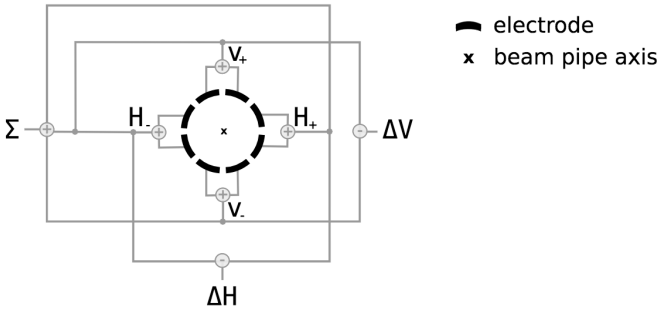

Figure 4.6: Inductive peak-up and scheme of signal treatment. 8 electrodes are assembled around the beam line axis. The signals picked up by each one of them are summed in pairs and then again combined and subtracted to produce one sum (Σ) and two difference (Δ) signals [16].

BPI are appreciated for their large bandwidth and for the fact that all the sensitive parts of them are located outside of the vacuum [15].

4.2 Cavity BPM description

Six cavity BPMs have been initially dispersed along the injector. The study presented only consider 5 of them, as depicted on Figure 4.7. They are referenced following the same numbering as for their inductive counterparts and all the accelerator equipments on CLEAR. The studied cavity BPM are numbers 220, 240, 260, 310 and 380.

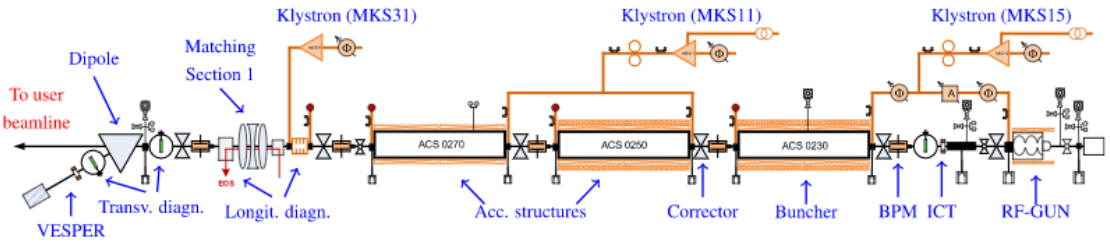

Figure 4.7: Location of the cavity BPMs studied along CLEAR injector.

Cavity BPMs act as resonant cavities. RF signals detection and processing is done by the associated electronic system.

4.2.1 Hardware description and functioning

CLEAR cavity BPMs are coaxial re-entrant cavities, made in titanium and as compact as possible. Their principle is based on excitation of electromagnetic fields (corresponding to resonant modes) when bunches pass through. Four antennas are orthogonally located on the top, bottom, left, and right transverse locations of the cavity, and pick up the RF signals. The design of CLEAR's cavity BPMs is depicted in Figure 4.8, and the resonant modes are illustrated in Figure 4.9.

Two main modes, that correspond to Bessel functions of different orders, both transverse magnetic, can be excited by the beam passage:

- A monopole TM_{010} mode (in dark blue on Figure 4.9), proportional to the beam intensity and does not depend on the beam position,

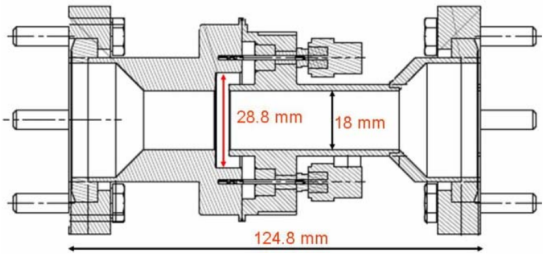

Figure 4.8: CLEAR cavity BPMs design [17].

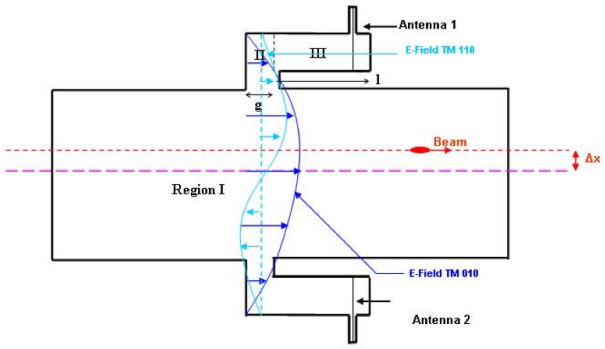

Figure 4.9: Scheme of the geometry and modes of a re-entrant cavity BPM. The geometry 3 main distinct parts are the beam tube (I), the gap (II), and the coaxial cylinder (III) [18].

- A dipole TM_{110} mode (in light blue on Figure 4.9), proportional to the distance of the beam from the center axis of the monitor and the beam intensity.

Other modes of excitation are negligible in comparison with these two polarizations. The output voltage V_{out} with an impedance Z is given in Equation 4.1, where R/Q is the shunt impedance, q the bunch charge and ω_i is the mode frequency. The beam intensity is directly linked to the bunch charge q as reminded in Equation 4.3, where t and l respectively represent units of time and length, and β the ratio of the particles velocity to the speed of light c. Both modes (monopole and dipole ones) output voltages depend on the beam intensity. However the shunt impedance of the monopole mode is constant, whereas for the dipole mode, it is proportional to the beam transverse offset.

For each mode, the resonant frequencies have been measured and averaged over the 6 BPMs used on CLEAR, and the results are given in Equation 4.2 (more details can be found in Reference [17]). The dipole mode frequency ω_2 has been considered for a resonant operation with 32 bunches. The cavity design has been done in order to ensure a large frequency separation between the two cavity main modes; the wavelengths of the resonator modes are fixed by the cavity dimensions, due to boundary conditions of electric field at the walls. RF signals are sent from the antenna to an electronic system in order to return the desired beam parameters.

$$V_{out} = \sqrt{\frac{\omega_i^2 (R/Q) q^2 Z}{Q_{ext}}} \tag{4.1}$$

$$\omega_1 = 3990\ MHz \qquad \omega_2 = 5985\ MHz \tag{4.2}$$

$$I\,[A] = \frac{q}{t} = \frac{q}{l} \cdot \beta c \tag{4.3}$$

4.2.2 Signal acquisition

The signals treatments is more complex than for inductive BPMs, namely due to issues for the separation signals from the two excited modes. For small transverse displacements of the beam (in µm range), the dipole mode is weakly excited whereas the monopole mode is strongly expressed. A method in 3 steps is applied to isolate TM_{110} mode signal.

The signal processing electronics are described in Figure 4.10. Directly inside the machine tunnel, the signals issued from the 6 BPMs are combined with hybrid couplers connected to each pair of opposite antennas (in pink on Figure 4.10 and depicted in Appendix A.1.1) that provides sum Σ and difference Δ signals. It performs an isolation higher than 18 dB in the range of 2 to 8 GHz, rejecting a wide part of the noise.

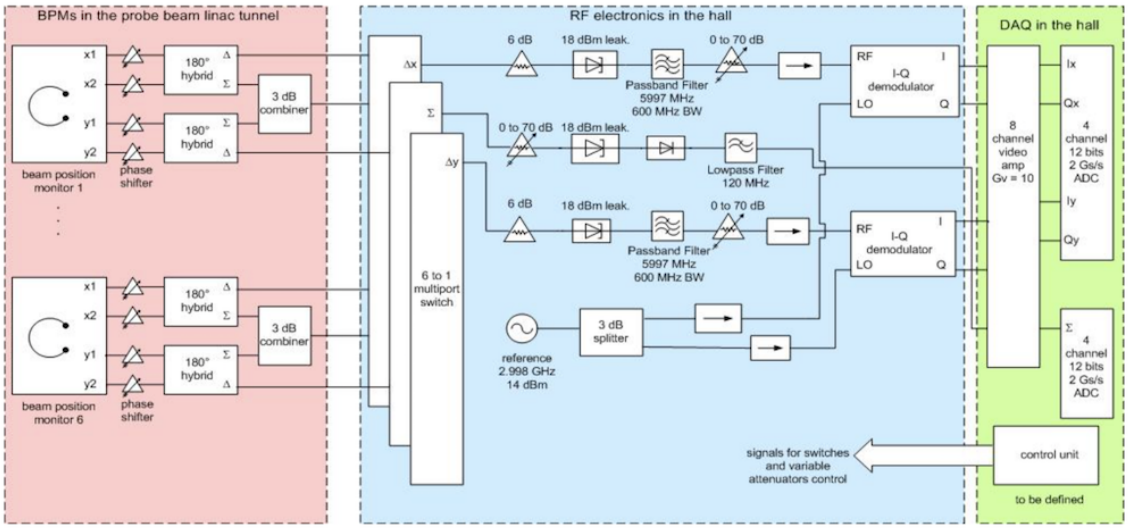

Figure 4.10: Signal processing electronics [17].

The out coming signals are connected in parallel to two identical electronic crates [19] (in blue on Figure 4.10 and depicted in Appendix A.1.2) located in the gallery, that allow simultaneous read-out of two BPMs. The crates are equipped with RF switches and adjustable attenuators. A first switch selects the BPM to connect, and the chosen signals are then derived to obtain as outputs a rectified Σ, and I/Q signals [20].

During this second step, Δ signals pass through 600 MHz bandwidth bandpass filter centered on the dipole mode frequency. A reference signal at the LINAC operation frequency of 2.998 GHz is then used for the I/Q modulation, carried out for the synchronous detection of the dipole signals. This acts as the third step of the TM_{110} mode signals isolation.

Σ, I_x, I_y, Q_x, and Q_y signals are then sent to acquisition boards for analog to digital conversion. The amplitude of the dipole mode gives the beam displacement from the cavity center, and its phase the sign of the displacement. The phases and amplitudes of the two modes are processed, and the phase of the dipole mode is reconstructed from the phase of the monopole mode.

In parallel of this signal treatment, the monopole mode signal is also accessible from a Shottky diode located in parallel to the electronics crates (before the blue part on Figure 4.10). The combined Σ signals first meet a splitter when arriving in the hall. One output of this splitter goes to the described circuit and the other enters in a diode, that acts as a rectifier and low pass filter. The train intensity can also be studied from this signal.

Cavity BPMs are appreciated for their good time (2.8 ns damping and rising times) and position resolutions, the latter being due to the position sensitivity lead by the cavity shunt impedance. The simplicity the design of cavity BPMs allows a high precision of their machining and in the modes frequencies chosen. For these reasons their utilization was studied on the CLIC test facility, lepton colliders requiring a high precision on beam position. They now need to be recalibrated for CLEAR's beam.

4.3 Data acquisition

Some data were taken before CLEAR summer 2018 shutdown in order to start the BPMs calibration. A first focus was driven on their responses with the beam train charges, which is directly linked to the beam current (cf. Equation 4.3).

The time structure of electron bunches traveling in CLEAR is described in Figure 4.11. Electrons are

extracted thanks to a laser pulsing the photo-cathode at a 1.5 GHz frequency, and bunches are shaped thanks to the RF-gun and the buncher. Trains made of a tunable number of bunches periodically repeat at a repetition rate adjustable between 0.855 and 10 Hz.

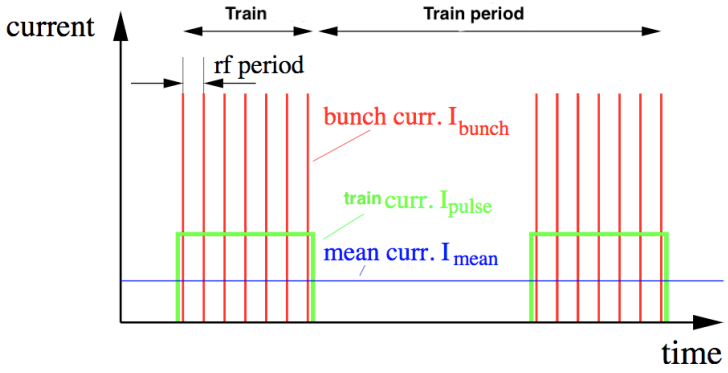

Figure 4.11: Time structure of the different currents at a pulsed LINAC.

The charge per train can be adjusted using two methods. One consists of changing the number of bunches per train, and the other the charge per bunch. The number of bunches per train can be tuned thanks to two Pockel cells that can restrict when, within the train, the laser pulses are actually hitting the cathode. Regarding the charge per bunch, it is adjustable by tuning the laser power. Below a saturation phenomenon that will be observed in Section 4.4.1, a cathode hit with a bigger laser energy will eject more electrons.

In order to calibrate first the charge measurement of all the BPMs, data have been taken varying the bunch charge and the number of bunches, with the aim of first understanding the BPM's behaviors with respect to the beam trains structure. For each measurement, the train charge was also acquired with the Bunch Length Monitor located after the RF-gun and next to the first cavity BPM. This device is a well known Integrating Current Transformer (ICT, indicated on Figure 1.2). It is calibrated and gives a trustful value of the train charge. However, since it is mounted close to the gun, it will include a larger contribution from dark current.

4.4 Results analysis

The goal of the following work was to focus on the beam charge detection for all BPMs. Both mentioned possibilities of charge increase have been studied. The data have been taken and analyzed developing Matlab scripts. In this section, the charge increase scale made from the reference ICT is first explained, then are shown the results of BPMs behavior for each charge increase mean, and behavior of some BPMs signals are then confronted with both means.

4.4.1 Charge increase

Figures 4.12 and 4.13 show the train charge measured with the ICT at the output of the gun for both means of charge increase. For each charge setting, 5 measurements have been taken and averaged. Error bars have been determined with the standard deviation of these 5 values, which increases with the train charge.

From the raw signal plotted in Figure 4.13, a charge offset of 4.7 ± 0.3 pC per train is measured at "0 bunch" (no hit of the laser). This current is due to the high fields in the RF-gun, that can generate field-emitted electrons from the cathode. Transported downstream the accelerator, these electrons form this so-called dark current and it should not be taken into account for the train charge measurement. This 4.7 ± 3 pC value has been subtracted from the train charge scaling for the rest of the study.

In the same way, the dark current seen on Figure 4.12 has been removed for the rest of the study. This one

has a bigger value of 8.8 ± 0.2 pC, that may be due to the fact that even with the maximum laser attenuation, its energy is not down to 0 and some leakage may result from the 10 pulses.

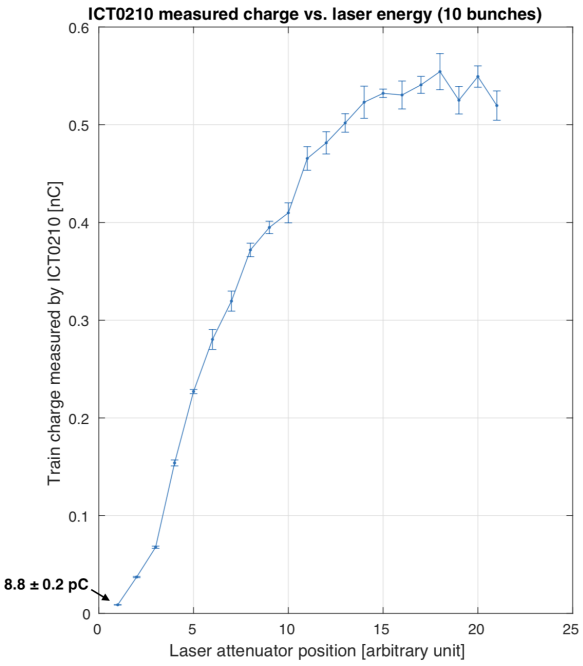

Figure 4.12: Train charge evolution with laser energy increase for 10 bunches.

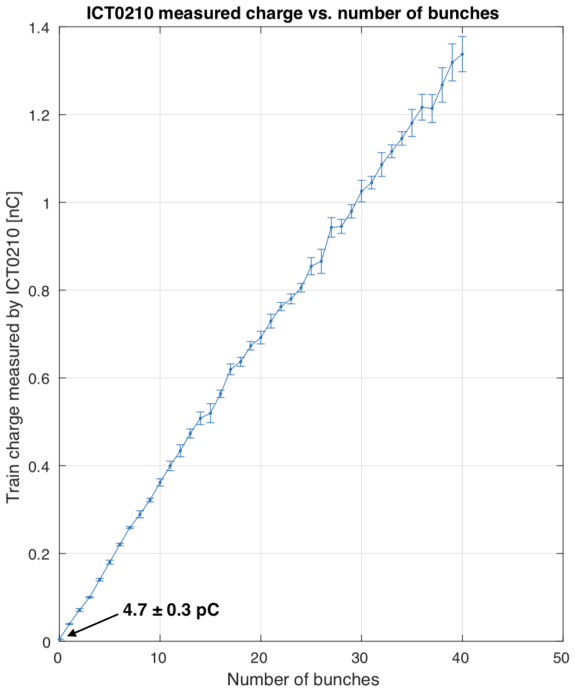

Figure 4.13: Train charge evolution with number of bunches increase (0 to 40 bunches).

Considering Figure 4.12, we observe a saturation of the measured train charge above 532 ± 4 pC, corresponding to 53.2 ± 0.4 pC/bunch. Above a certain energy, a laser hit on the cathode reaches a maximum amount of particles that it can extract. However below this limit, the ICT shows a feasible rise of the measured current. This curve of the measured charge below 532 ± 4 pC perfectly follows shape of the one of the laser energy. The irregularities do not come from the ICT, but from non linearity between the attenuator position and the laser energy. For the next analysis, data taken above 532 pC train charge (14^{th} laser attenuator setting) with the laser power increase will not be considered.

Figure 4.13 shows a linear rise of the measured train charge and reveals a bunch charge of 35 pC for this measurement.

For both ways of train charge increase, these measurements will be considered as a reference scale to calibrate the BPMs.

4.4.2 BPMs behavior with charge per bunch increase

BPMs responses have been acquired for inductive BPMs sum signals and cavity BPMs Shottky diode and final Σ signals. Results are presented per BPMs type sets and for each signal type. The data taken from the Δ signals will not be studied here.

Inductive BPMs

The sum signals from the inductive BPMs (cf. Appendix A.2.1) appear to show between one and two negative peaks with the absolute maximum value rising with the bunch charge. The shape instability with the bunch charge may come from the fact that signals have been acquired with a low time resolution sampler, and for each sample, only a few points are taken at the peak location.

The most convenient parameter to follow the beam increased was found to be the maximum peak absolute value. Figure 4.14 shows the plot of this parameter versus the train charge increase for all inductive BPMs.

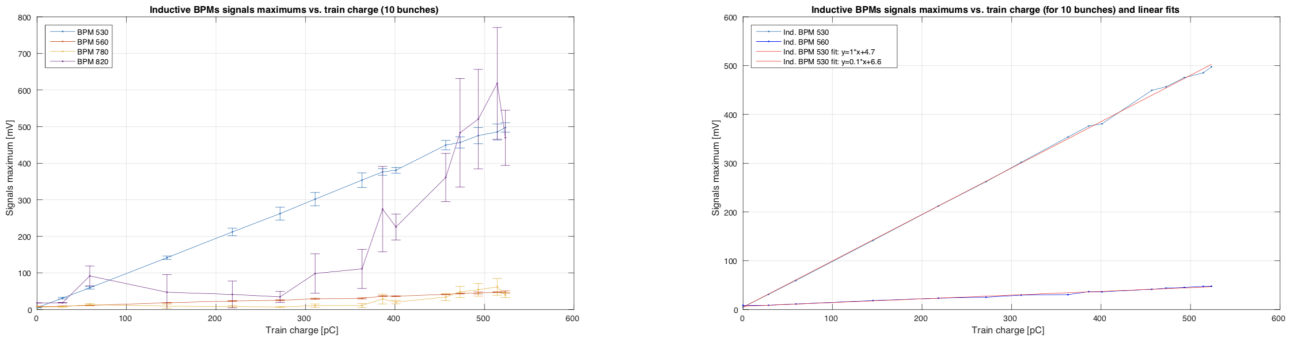

Figure 4.14: Inductive BPMs signal absolute maximum as a function of the charge increase and fit for BPMs 530 and 560.

Only BPMs 530 and 560 show a linear behavior with train charge increase. The fitting curves are shown on the figure at the right. BPM 530 demonstrates a larger response. Its resolution has been improved recently. Sensitivity of BPM 560 should also be improved soon, as a controllable gain system will be installed for all inductive BPMs. BPM 780 shows no signal evolution below about 350 pC per train, and error bars for higher charges are too large to allow making conclusions. Its sensitivity should be improved too. The errors bars reveal an unstable beam at the end of the beamline, when the data were taken. For this reason, the calibration of BPM 820 was not possible with this data set.

Cavity BPMs diode signals

Figure 4.15 shows the oscillating sum signal of the cavity BPM extracted via the Shottky diode, set up as described in Section 4.4.2. The oscillation amplitude rises with the bunch charge increase. Plotted versus the train charge increase in Figure 4.16, the signal's amplitude is a relevant parameter to reflect the train charge elevation until at least 500 pC.

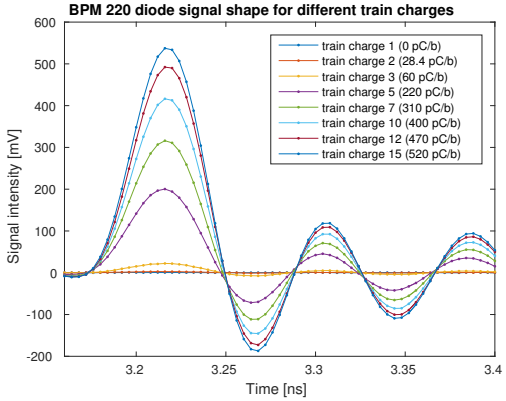

Figure 4.15: BPM 220 Σ signals read from a diode for different bunch charges.

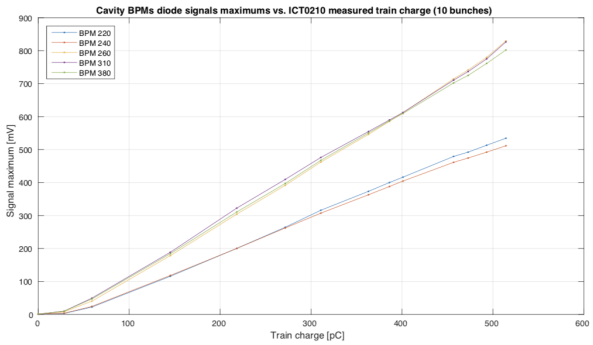

Figure 4.16: Cavity BPM Σ signals evolution with train charge increase tuning the bunch charge via the laser power attenuator.

This behavior is however not perfectly linear below 30 pC. The diode signals for the two first train charges (below 30 pC) are flat. This may be due to a small threshold of the diode. The extraction of the Σ signal using the RF treatment (detailed in Section 4.2.2) may avoid this problem.

Cavity BPMs sum signals

As a matter of example, the Σ signal of BPM 260 has been acquired at the end of the two electronics, called ELN1 and ELN2, to ensure that those are processing the signals in the same way. The signals observation actually reveals different behaviors of the two electronics. Signals from ELN1 shows a single positive peak response, whose amplitude increases with the charge, whereas ELN2 shows a peak of opposite sign, followed by oscillations. Appendix A.2.2 shows the shape of these signals.

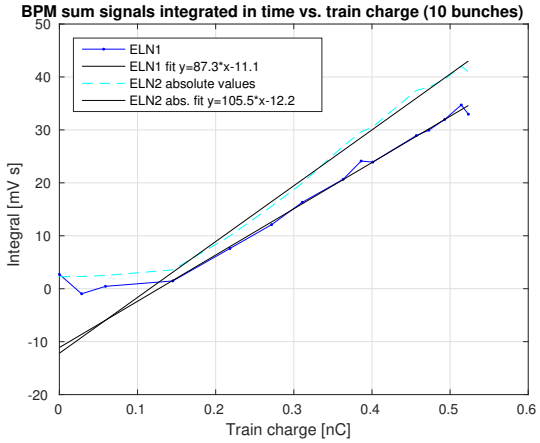

Figure 4.17: Cavity BPMs sum signals out of the 2 electronics (ELN1 and ELN2) integrated in time, as a function of the train charge.

The absolute maximum of these peaks has been plotted on Figure 4.17 versus the train charge. Seen from this parameter, both signals have a linear behavior with the charge increase above 150 pC. The linear fits applied for the data taken above this limit are shown on the graph and their equations appear in the legend.

Conclusions

Considering the train charge increase when tuning the laser power attenuator, inductive BPMs 530 and 560 have been calibrated for their charge measurements for charges up to 500 pC per train. The second has a lower dynamic, but its sensitivity should be improved soon. The calibration of the two others inductive BPMs was not possible with this data set due to bad transport of the beam.

Sum signals of the cavity BPMs have been studied first in their "raw" state, before the RF processing step, thanks to a Shottky diode inserted before the RF signal processing. All BPMs show a linear behavior with the train (and bunch) charge increase, except for low charges. This may be due to the presence of a small diode threshold. This first study of the Σ signals proofs that the charge measurements can be calibrated properly for all the BPMs of this type that are installed on CLEAR, at least above 30 pC train charge.

The cavity BPM Σ signals after RF rectification have been calibrated with the train charge increase due to bunch charge augmentation. However, this calibration only works for train charges above 100 pC, and the poor sensitivity for low charges previously observed with the diode does not improve with the signal treatment operated by the RF crates. Once they will be calibrated and their resolution improved, inductive BPMs may be used for small charges detection (below tenths of pico-Coulombs) [12].

4.4.3 Behavior of BPMs with increasing number of bunches

In the same way, the BPMs behavior have been investigated when the train charge increases via the number of bunches, considering trains between 0 and 40 bunches. With this method, the BPMs response could be studied for train charges up to 1.4 nC (whereas the previous measurements done with 10 bunches lead to a saturation of the photocathode at 500 pC). All the signals have been extracted and treated in the same way, meaning that for the BPM response examination, the choice of considering the signal peak or the signal integrated over time has been repeated for this study. Error bars when available were also similarly determined.

Inductive BPMs

Figure 4.18 shows the plot of inductive BPMs response the train charge, with the number of bunches growing from 0 to 40.

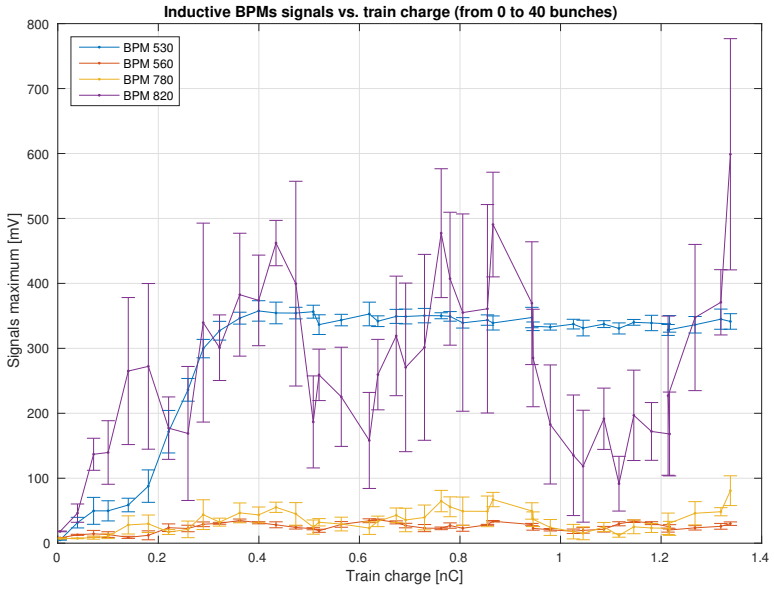

Figure 4.18: Inductive BPMs signals peak as a function of the train charge, for a bunch number increase (0 to 40 bunches).

Due to a bad beam transport at the end of the experimental line, data taken from BPM 820 could again not be interpreted, as witnessed by the large error bars. BPMs 560 and 780 don't show any exploitable response with the large scale charge increase. Considering the scale of charge increase, this may not be due to a bad resolution or sensitivity this time. Only BPM 530 shows an exploitable response. This response is not linear but still increase with the train charge. The signal saturates above 400 pC of train charge. The tunable gain system that will be installed should solve this issue. Measurements should be made again once the system has been installed to do the calibration.

Cavity BPMs diode signals

The cavity BPMs Σ signals detected by the Shottky diode don't behave as linearly with the bunch number as with the bunch charge. Figure 4.19 shows that the signal intensity increases with the train charge, but only the two first BPMs show a really linear behavior, and this above 500 pC of train charge (range that was not accessible when considering bunch charge increase with 10 bunches). The associated fits are shown in Figure 4.20.

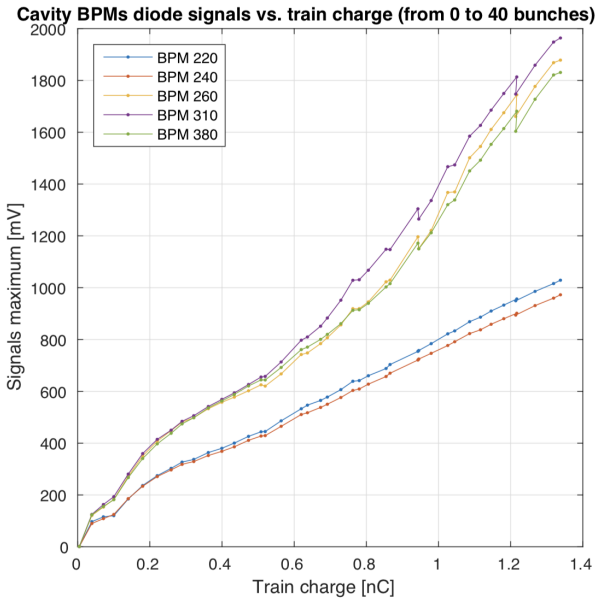

Figure 4.19: Cavity BPMs signals maximum versus the train charge for 0 to 40 bunches.

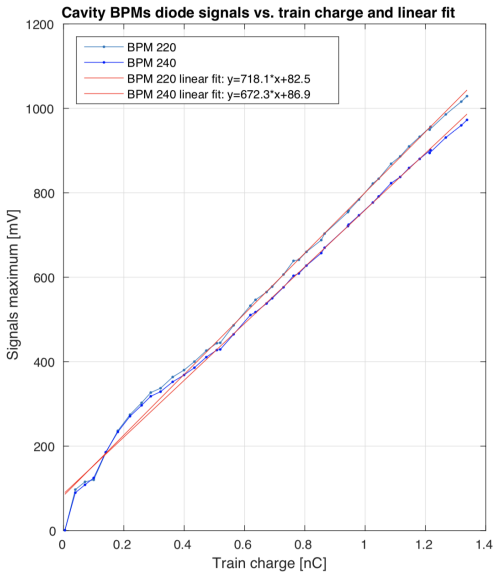

Figure 4.20: Linear fit to the oscillation amplitude of the BPMs 220 and 240 Σ signals filtered by the diode, plotted versus the train charge, for 0 to 40 bunches.

For low train charges, this diode-filtered signals show sudden slope changes. A dedicated program based on a circuit model and written in Python was used as simulation tool to study the cavity signals superposition for several bunches passing at a 1.5 GHz frequency. The bunches were simulated as passing through the center of the cavity in order to focus on the monopole mode. Figure 4.21 shows the results obtained.

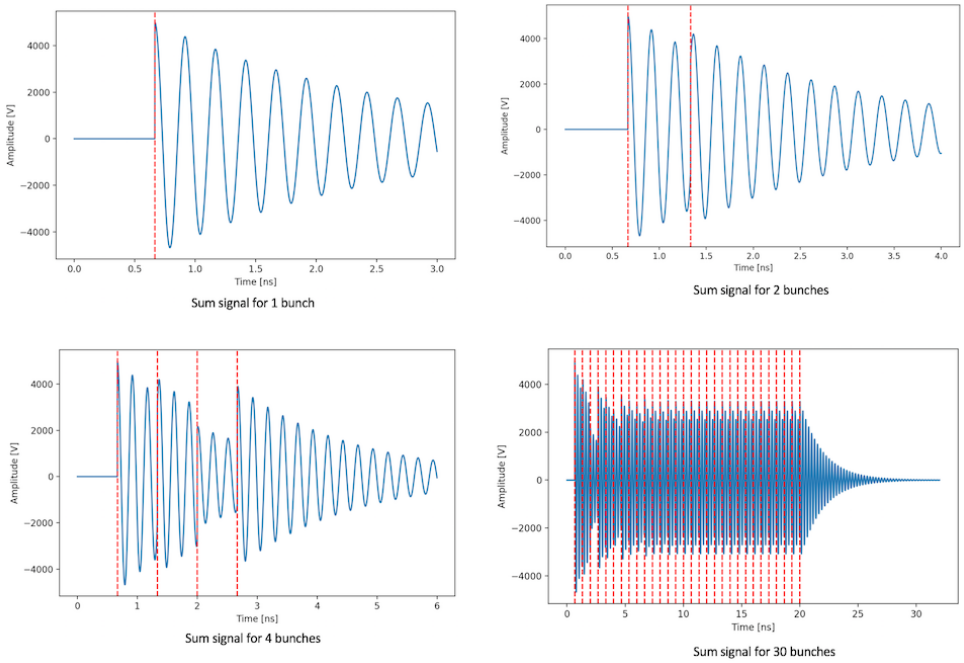

Figure 4.21: Simulation of the cavity response signals for 1, 2, 4 and 30 bunches passing through its middle with a bunch space of 1.5 GHz. Bunches are indicated with vertical red dots lines.

The top right graph shows destructive interferences between the signal issued from the monopole mode excitation by the first bunch, and the signal generated by the second bunch passage. The bunches passage frequency of 1.5 GHz is indeed not a multiple of the monopole mode frequency, corresponding to 3.99 GHz.

The third bunch passage also leads to a destructive interference, but the fourth bunch passage results in a constructive one. The simulation of 30 bunches, represented on the bottom right graph, reveals a monotony in the resulting amplitudes, starting after seven bunch. Considering that the diode acts as a rectifier followed by low pass integrating filter with this signals, the changes of slopes noticed on Figure 4.19 after the 3 bunches train comes from fact that the mode and bunch passage frequency are not multiples. Cavity BPMs will not allow good measurements in the cases of a small number of bunches.

The 2 teeth peaks noticeable on the BPMs 260, 310 and 380 around 870 pC and 1210 pC seem to be related to two consecutive measurements taken with the same number of bunches as revealed by horizontal steps for these train charges values on Figure 4.13. Beam instabilities, due to the decreasing quality of the transport along the line at the moment of the acquisition of these data, explain why this is only visible for the BPMs the most distant from the cathode (the 2 points are superposed on the two first BPMs curves). The same plot versus the number of bunches, shown in Appendix Section A.2.3, confirms this explanation.

Cavity BPMs sum signals

The Σ signals processed by both electronic crates are shown in Figure 4.22. Those that passed by ELN1 show a signal of which the integral over time increases with the train charge. Signal coming from ELN2 however oscillates in time and the maximum amplitudes of the peaks coming after the first one can be higher (than the first peak amplitude), as shown by the red arrow. The amplitude of the first peak also does not increase with the bunch number. Finding a parameter on this signal to determine the beam current seems complicated. Signals from both integrated over time to calibrate the current determination for number of bunches increase. The given results depicted on Figure 4.23 were predictable from the signal shapes: electronic crate ELN1 provides a signal of which the integral over time rises linearly with the train charge above 100 pC. The threshold of poor sensitivity for low charges is still present. Integrated signals from ELN2 don't give any correlation with the train charge. Considering the maximum of the signal would not be more relevant, given its fluctuation.

To determine what is wrong with the ELN2, I/Q signals of both axis x and y have been studied independently and compared between the two electronics. The problem may come from an inversion of two of those signals in one of the connection. This investigation is ongoing.

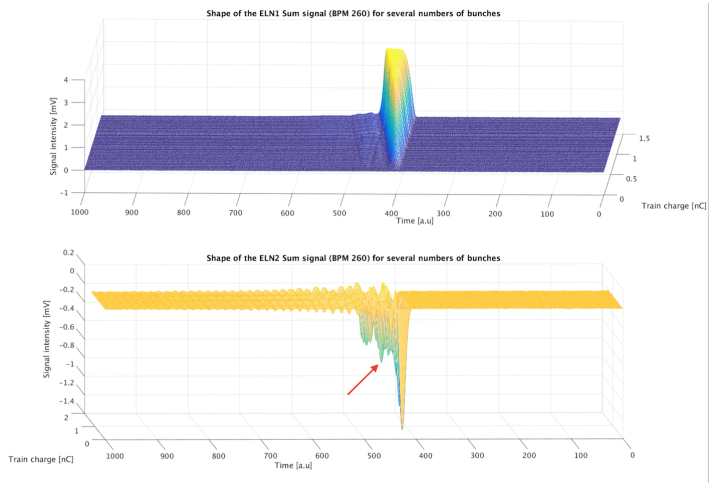

Figure 4.22: Cavity BPM 260 signal shape with train charge increase (time has to be read from right to left), for the two RF crates ELN1 and ELN2. The red arrow shows a peak arriving after the first big one, and that has a bigger amplitude.

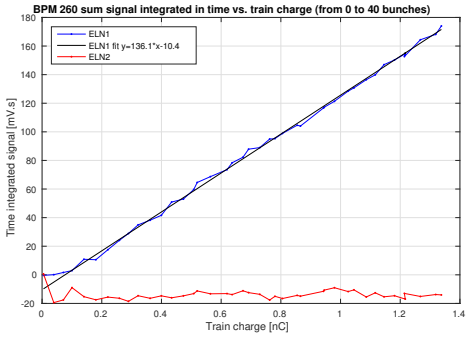

Figure 4.23: Comparison of ELN1 and ELN2 RF processing, to calibrate BPMs Σ signals with the train charge.

Conclusions

From the data taken increasing the number of bunches, no calibration has been done for the inductive BPMs. The only exploitable signals were those of BPM 530. This BPM shows a linear increase from 200 to 300 pC and saturates for higher train charges. A linear fit of its data below 300 pC showed a similar increase as observed with the laser energy increasing for such train charges. In summary, such data may be taken again to calibrate inductive BPMs once their electronics will have been modified and gain will be controllable. The final goal is to reach sensitivity for low charges, down to below tenths of pico-Coulomb.

Sum signals of the cavity BPMs extracted by the diode reveals non linearities for a low number of bunches, due to the interference of the bunch generated signals. Above about 15 bunches, BPMs show a good linearity with the charge increase and calibrated curves have been computed for train charges above 15 bunches for the two first cavity BPMs.

The sum signal out of the ELN1 has also been calibrated with good results, above 3 bunches (100 pC train charge). More data should be taken to study with more statistics the difference of slope obtained between the two calibrations.

This cavity BPM still shows a poor sensitivity to low charges. ELN2 signal must be investigated, it does not look usable for the moment. No explanation was found to explain that it was possible to calibrate its output for bunch charge increase and not for increasing bunch numbers.

Finally, inductive BPMs are appreciated for their good sensitivity with low charges, and cavity BPMs for their ability to measure high charges. Once BPM sum signals will have been calibrated with the charge, Δ signals will be investigated and the position measurement from the BPMs will be calibrated the measured displacement when steering the beam upstream.

Conclusion

CLEAR beam parameters are lead by the experiments taking place on the facility. For a best control of these parameters, beam diagnostics need to be set up and mastered all along the LINAC and the experimental beamline. Improvement of the beam diagnostics have been performed during spring and summer 2018.

A new software has been implemented to ensure a fast, precise, and error-prone measurement of the bunch length, using the dedicated deflecting cavity. The programs have been organized to permit their libraries to be reused for other software development. The GUI implementation and test by both machine operators and external users were successful. Some improvement have been made thanks to this testing period, concerning as well the data treatment as the GUI display. Some of its limits have been discussed and shared, and some improvement can still be made, namely concerning measurements of compressed bunches.

The computations required for the two dipole spectrometers calibration have been achieved. The results obtained reach the operators expectations in terms of precision, and the two spectrometers are complementary with the energy scales that they can measure at the output of the LINAC and at the end of the main experimental beamline.

The calibration of the two sets of inductive and cavity BPMs that are installed along the machine has also started. Only the calibration of their sum signals, that must be calibrated with the beam charge, has been discussed yet. The electronics of both monitor types need to be improved to reach better results. In the case of inductive BPMs, a system of tunable gain will be installed, with the aim of reach a good sensitivity with low charges. In the case of the cavity monitors, the complex RF signal processing sometimes lead to non exploitable signals. However their behavior study with increasing number of bunches proofed their linearity with train charge increasing up to 1.4 nC. Once Σ signals will have been calibrated, the Δ ones, correlated with the beam transverse position will be investigated, and they will become fully operational, in particular for orbit studied.

CLEAR machine shutdown will end at the beginning of September 2018, and the new tools developed are operational for the arrival of the first users.

Bibliography

[1] CLEAR official website: https://clear.web.cern.ch/.

[2] D. Gamba, R. Corsini, et al.,
The CLEAR user facility at CERN,
Nuclear Instruments and Methods in Physics Research, Section A: Accelerators, Spectrometers, Detectors and Associated Equipment, December 2017.

[3] Aicheler M., Burrows P., et al.,
A Multi-TeV Linear Collider Based on CLIC Technology: CLIC Conceptual Design Report, Tech. Rep.,
CERN-2012-007, CERN, Geneva (2012).

[4] A. Mosnier, et al.,
The probe beam linac in CTF3,
Proc. 10th European Particle Accelerator Conf. (EPAC2006), Edinburgh, UK, pp.679-681, 2006.

[5] Ross I.N.,
Feasibility Study for the CERN CLIC Photo-Injector Laser System, Tech. Rep.,
CLIC-Note-462, CERN, Geneva, Switzerland (2000).

[6] C.A. Lindstrøm, E. Adli, et al.,
Emittance Preservation in an Aberration-Free Active Plasma Lens,
August 2018.

[7] C.A. Lindstrøm, K.N.Sjobak, et al.,
Overview of the CLEAR plasma lens experiment,
Nuclear Instruments and Methods in Physics Research Section A: Accelerators, Spectrometers, Detectors and Associated Equipment, January 2018.

[8] S. Deghaye, E. Fortescue-Beck,
Introduction to the BE/CO control system,
2016 Edition.

[9] Git repository of the bunch length measurement software implemented on CLEAR in 2018: https://gitlab.cern.ch/CLEAR/DeflectorControl.

[10] Magnet ID card: PXMCXCAHWC-DA000089: https://norma-db.web.cern.ch/magnet/idcard/1331/.

[11] Patron, G et al,
Mesure magnétique d'un dipôle type MDX avec entrefer de 52 mm,
PS-PA-MA-Note-88-30.

[12] Personal communication, Wilfrid Farabolini, August 21st 2018.

[13] R. Bossart,
High precision beam position monitor using a re-entrant coaxial cavity,
Proceedings of the 1994 International Linac Conference, Tsukuba, Japan.

[14] Marek Gasior,
An inductive pick-up for beam position and current measurements,
Proceedings of DIPAC 2003.

[15] Peter Forck, Piotr Kowina, Dmitry Liakin,
Beam Position Monitors,
Gesellschaft fur Schwerionenforschung GSI, Darmstadt, Germany.

[16] A. Palaia,
Commissioning of inductive BPMs in the TBTS probe beam line,
CTF3-Note-106.

[17] C. Simon, et al.,
Beam Position Monitors using a re-entrant cavity,
Proceedings of DIPAC 2007, Venice, Italy.

[18] Claire Simon, et al.,
Performance of a reentrant cavity beam position monitor.

[19] C. Simon, et al.,
Instrumentation for high frequency cavity BPM in CALIFES,
Proceedings of PAC09, Vancouver, BC, Canada.

[20] National Instruments^{TM} website: http://www.ni.com/tutorial/4805/en/.

ANNEXES

A Appendix

A.1 Cavity BPMs electronics systems

A.1.1 Cavity BPMs hybrid coupler and combiner

The first part of the cavity BPMs electronics shown on Figure A.1 is located in the tunnel, close to the BPM cavities, and collects the raw signals coming out of the BPMs antennas (bottom of the picture). The blue boxes contains the hybrid couplers, and the gray component gathering the sum signals coming from the couplers is a 3 dB combiner. Output signals (top of the picture) are then directed to the gallery.

Figure A.1: CLEAR cavity BPMs first part of the electronic hardware: hybrid coupler and combiner.

A.1.2 Cavity BPMs electronic in the gallery

Figure A.2 shows the rack dedicated to cavity BPMs in the gallery. The two RF crates ELN1 and ELN2 shown on Figure A.3 are stored at the bottom of the rack (green rectangle on Figure A.2) and contain the RF processing components. Input signals from the tunnel are plugged on the SMA connections of the crates box (left of Figure A.3). They travel through the depicted circuit and exit from the LEMO connections. They are then directed to the data acquisition system located in the middle of the rack (red rectangle on Figure A.2).

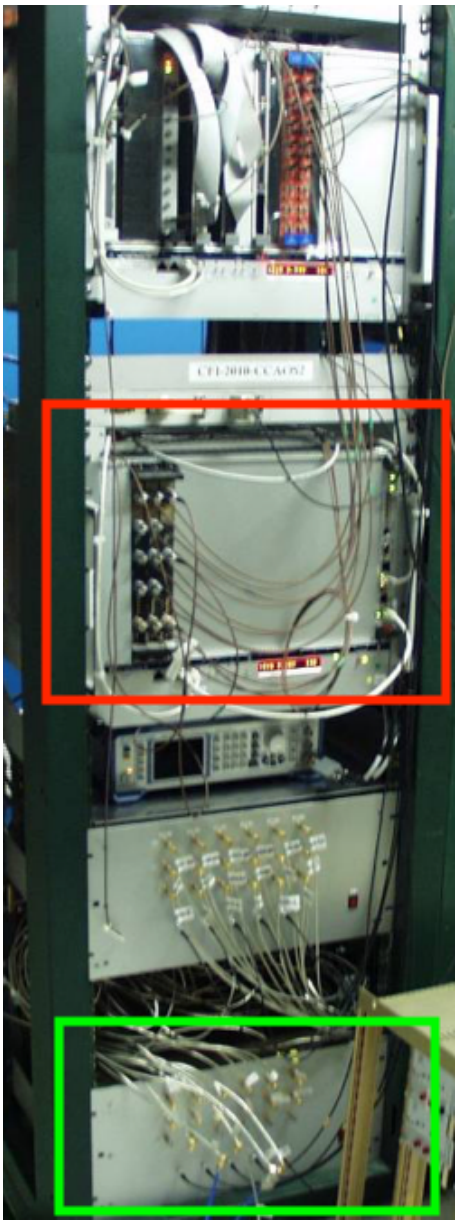

Figure A.2: Picture of the rack in the gallery dedicated to cavity BPMs signal processing. The green rectangle indicates the location of the RF crates and the red one, the data acquisition system, mainly operating the conversion of the analog signals to digitalized data.

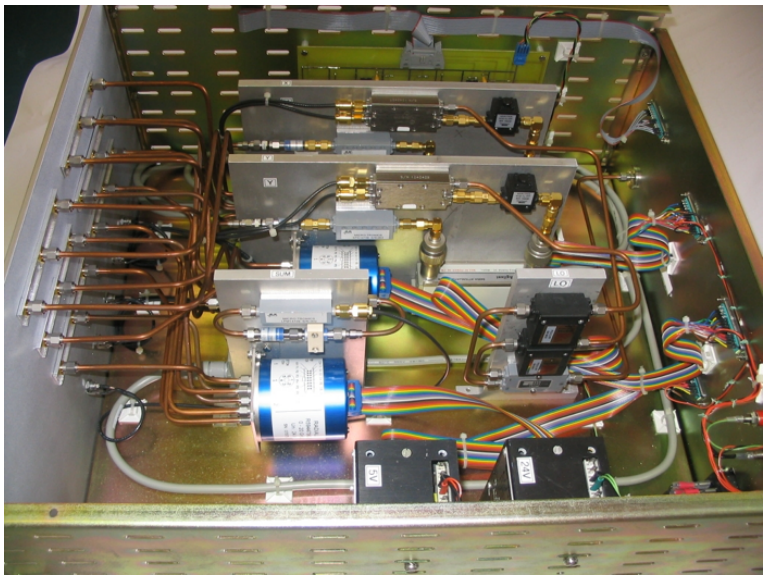

Figure A.3: RF crate processing signals coming from the cavity BPMs located in tunnel

A.2 BPMs Signals

A.2.1 Inductive BPM 530 signal response with bunch charge

Figure A.4 shows the shape of Σ signals from the inductive BPM 530, for different bunch charges. Their absolute maximum is rising with the bunch charge, even if the number of peaks also changes.

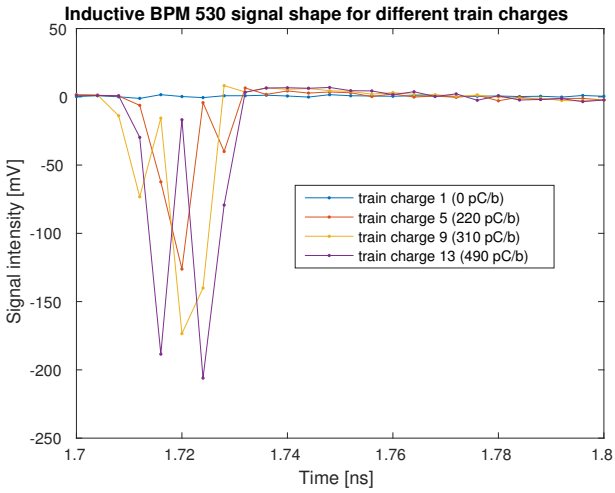

Figure A.4: Inductive BPM 530 signal shape for different bunch charges (10 bunches).

A.2.2 Cavity BPM 260 ELN1 and ELN2 signal responses with bunch charge

Figure A.5 shows the response of BPM 260 Σ signal with the train charge increase using the laser attenuator (with 10 bunches), for both RF electronics crates. Both cases show that the peak maximum increase with the train charge.

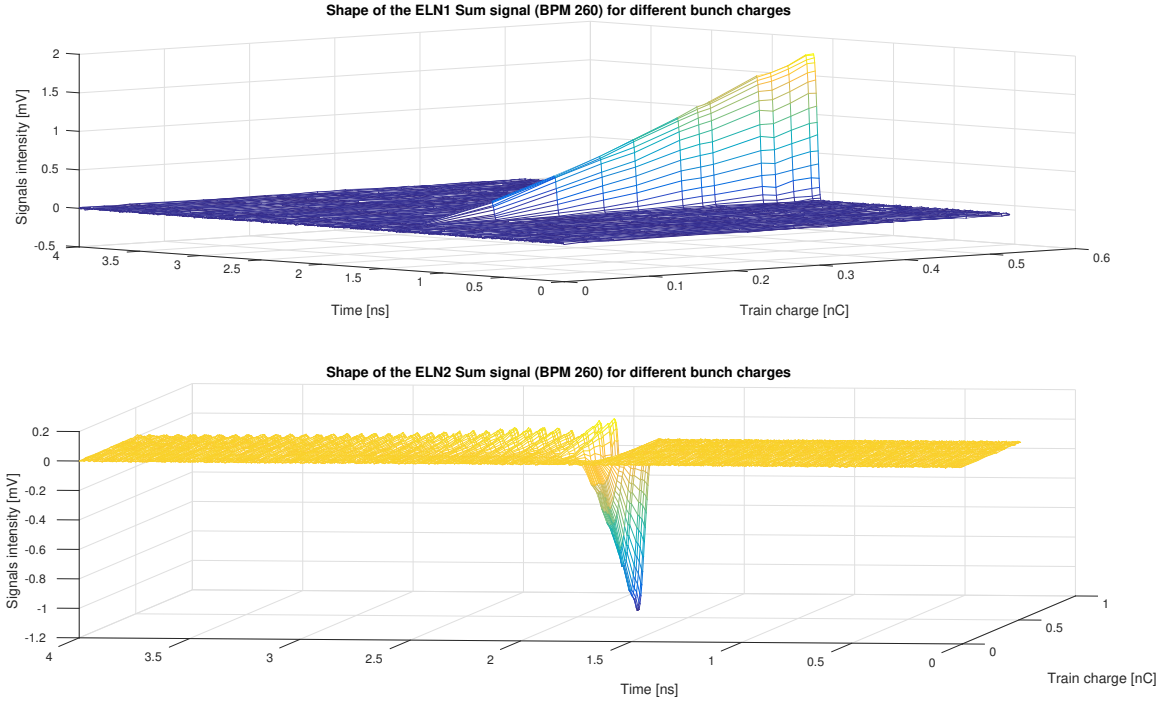

Figure A.5: Cavity BPM 260 signal shape with bunch charge increase (time to be read from right to left), for the two RF crates ELN1 and ELN2. The main peak maximum increase (in absolute value) with bunch charge is visible for the both electronics.

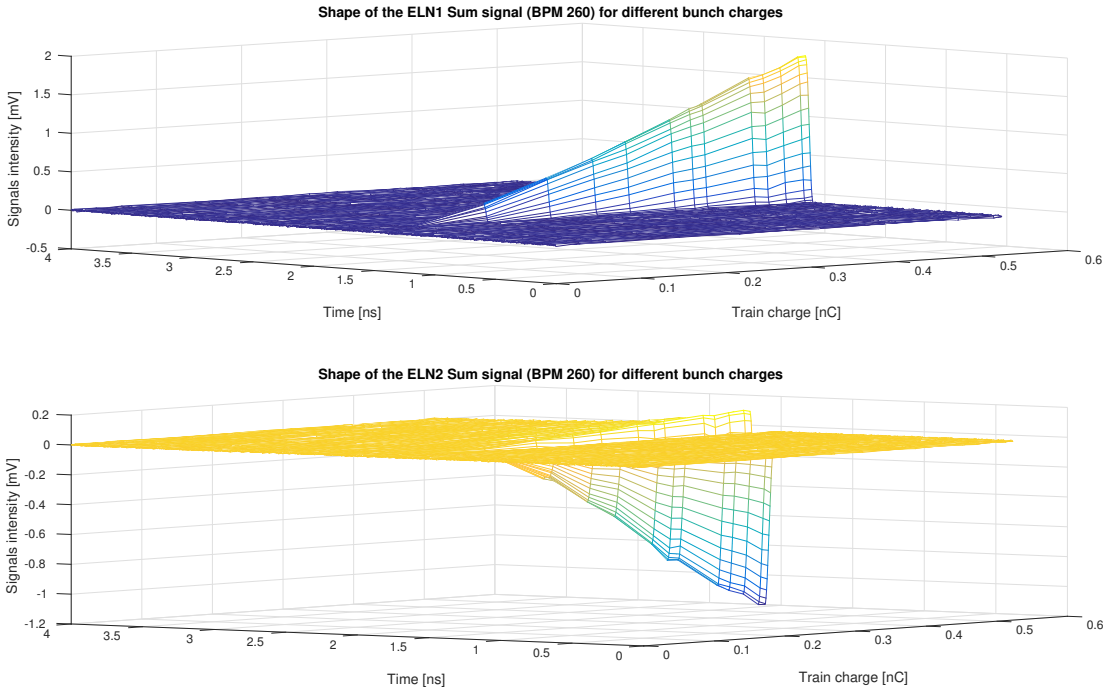

Figure A.6: Cavity BPM 260 signal shape with bunch charge increase (time has to be read from right to left), for the two RF crates ELN1 and ELN2. The oscillations following the main peak for signals coming out of ELN2 are visible on the bottom graph.

A.2.3 Response with the number of bunches, of the cavity BPMs signals filtered by the diode

Figure A.7 shows circled in red the consecutive measures taken with the same bunch number, clearly appearing as plateaus on on the 2 first BPM curves.

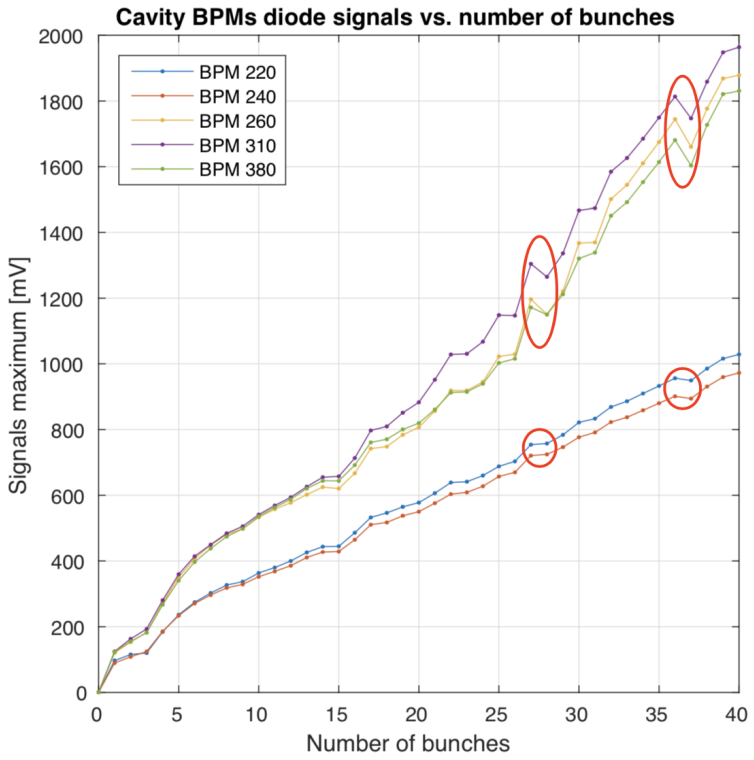

Figure A.7: Response with the number of bunches, of the cavity BPMs signals filtered by the diode.

Résumé

CLEAR (CERN Linear Electron Accelerator for Research), est un accélérateur linéaire d'électrons, expérimental, et basé au CERN. La grande variabilité des paramètres faisceau que peut fournir la machine attire des scientifiques de domaines variés, qui viennent réaliser leurs expériences sur les plateformes de test prévues à cet effet. Cette versatilité requiert un solide équipement en diagnostics faisceau. Différents diagnostics ont été implantés et calibrés durant la période de fonctionnement de la machine au printemps 2018 et de celle d'arrêt qui s'en est suivi.

Une nouvelle interface graphique a été implementée dans le but de réaliser des mesures de longueur de paquets à l'aide de la cavité déflectrice. Cet outil a été développé dans une philosophie durable, de sorte notamment à ce que ses librairies puissent être réutilisées pour le développement d'autres programmes. L'interface a été testée avec succès, à la fois par les opérateurs de la machine, et par les expérimentateurs présents. Ses limites ont été discutées et quelques améliorations doivent encore être apportées.

Les calculs nécessaires à la calibration des spectromètres sont décrits dans ce document. Les résultats obtenus sont à la hauteur des attentes des opérateurs en terme de précision. Les deux spectromètres sont complémentaires concernant les plages d'énergie qu'ils recouvrent et permettront, dès le redémarrage de la machine, de mesurer l'énergie du faisceau en sortie de l'injecteur, et au bout de la ligne expérimentale principale.

Les deux sets de moniteurs de position faisceau (à cavité et à induction) installés le long de l'accélérateur ont égalenent été etudiés. Leur calibration s'annonce complexe, mais ce document présente l'avancée de ce travail et les résultats déjà obtenus.

Abstract

CLEAR, the CERN Linear Electron Accelerator for Research is a stand-alone user facility located at CERN. Providing a wide range of beam parameters that allow s it to host a large spectrum of beam-based experiments, the machine also requires an important set of beam diagnostics. During 2018 spring beam time and summer shutdown, improvements have been performed to enlarge this set and improve its performance.

A new graphical user interface has been implemented in order to perform bunch length measurements using the deflecting cavity. This tool has been developed in a sustainable way, to permit its libraries to be used for other software developments. The software has been successfully tested by both machine operators and external users. Its limits have been discussed and some improvements can still be done.

The computations for the two energy spectrometers calibration are described in this paper. The obtained results have reached the users expectations in terms of precision, and the two spectrometers are complementary with the energy scales that they can measure.

The calibration of the two sets of beam position monitors (BPMs) that are installed along the machine have also started. This documents relates the investigation of the actual state of these BPMs setup.